universität wien

DIPLOMARBEIT

Titel der Diplomarbeit

The molecular function of tumor suppressor candidate 3 (TUSC3) and its role in prostate cancer

Verfasser

Erwin Tomasich

angestrebter akademischer Grad

Magister der Naturwissenschaften (Mag.rer.nat.)

Wien, August 2013

Studienkennzahl lt. Studienblatt:	A 441
Studienrichtung lt. Studienblatt:	Mikrobiologie und Genetik
Betreuerin / Betreuer:	Ao. Univ.-Prof. DI Dr. Natale-Erwin Ivessa

Table of Contents

Abstract

Prostate cancer is the most common diagnosed cancer in males in western developed countries. Many molecular aberrations can occur in the pathogenesis of this disease, though losses on the short arm of chromosome 8 are highly prevalent. Tumor suppressor candidate 3 (*TUSC3*) has been recently identified as a putative tumor suppressor gene in this region, but its precise molecular function is still elusive. TUSC3 shares high homology with a subunit of the oligosaccharyltransferase (OST) complex in yeast, hinting to a role in N-glycosylation. Indeed, we could demonstrate a physical interaction of TUSC3 with the catalytic subunit of the mammalian OST complex, STT3B. To unravel its role in prostate cancer progression, we downregulated *TUSC3* expression in prostate cancer cell lines DU145 and PC3 using shRNA mediated knockdown and analyzed them for their proliferative and carcinogenic properties *in vitro* and *in vivo*. We showed that loss of TUSC3 expression confers growth advantage to a prostate cancer cell line lacking Phosphatase and tensin homolog (PTEN) expression. Furthermore, we identified Protein Kinase B (AKT) activation as a mediator for proliferation and survival in these cells. We also observed increased migratory and invasive properties of prostate cancer cell lines upon TUSC3 knockdown. These findings were further supported by altered expression of two well-known adhesion molecules, E-cadherin (increased) and CD44 (decreased). For prospective studies, we provide first evidence that TUSC3 is linked to endoplasmic reticulum (ER) stress response. We found higher resistance to ER stress inducers and reduced expression of ER stress markers in TUSC3 silenced cells compared to control cells. Taken together, our findings demonstrate that loss of TUSC3 expression in prostate cancer cells has a detrimental influence on their tumorigenicity and that AKT displays a promising target in prostate cancer therapy.

Zusammenfassung

Prostatakrebs ist die häufigste Krebserkrankung bei Männern in den westlich-entwickelten Ländern. Viele molekulare Aberrationen treten in der Pathogenese dieser Krankheit auf, wenngleich Verluste auf dem kurzen Arm von Chromosom 8 am häufigsten sind. Tumorsuppressor Kandidat 3 (*TUSC3*) wurde als vermeintliches Tumorsuppressorgen in dieser Region identifiziert, jedoch bleibt seine genaue molekulare Funktion weitestgehend ungeklärt. TUSC3 weist hohe Homologie mit einer Untereinheit des Oligosaccharyltransferase (OST)-Komplexes in der Hefe auf, wodurch sich auf eine Rolle in der N-Glykosylierung schließen lässt. Tatsächlich konnten wir eine physische Interaktion von TUSC3 mit der katalytischen Untereinheit des OST-Komplexes, STT3B, demonstrieren. Um die Rolle in der Prostatakrebsprogression zu untersuchen, haben wir die Expression von TUSC3 in den Prostatakrebszelllinien DU145 und PC3 unter Verwendung von shRNA induzierter Hemmung herunterreguliert und analysierten sie auf ihre proliferativen und karzinogenen Eigenschaften *in vitro* und *in vivo*. Wir konnten zeigen, dass der Verlust von TUSC3 Prostatakrebszellen ohne Expression von Phosphatase and tensin homolog (PTEN) einen Wachstumsvorteil verleiht. Ferner haben wir die Aktivierung der Protein Kinase B (AKT) als Mediator für die verstärkte Proliferation und das Überleben dieser Zellen ausfindig gemacht. Wir beobachteten auch erhöhte Migration und Invasion in den Prostatakrebszellen mit niedriger TUSC3 Expression. Als Erklärung, fanden wir eine veränderte Expression der zwei Adhäsionsmoleküle E-Cadherin (erhöht) und CD44 (erniedrigt). In Hinblick auf weiterführende Untersuchungen gelang es uns, erste Hinweise auf eine Verbindung zwischen TUSC3 und endoplasmatischen Retikulum (ER) Stress zu gewinnen. Wir konnten zeigen, dass Zellen ohne TUSC3 und PTEN Expression widerstandsfähiger gegen ER Stress Induktoren sind und geringere Expression von ER Stress Markern aufweisen. Zusammengefasst zeigen unsere Ergebnisse, dass ein Verlust von TUSC3 in Prostatakrebszellen nachteilige Auswirkungen auf deren karzinogene Eigenschaften hat und AKT einen

vielversprechenden Angriffspunkt für eine mögliche Therapie im Prostatakarzinom darstellt.

1 Introduction

1.1 Prostate Cancer

1.1.1 Epidemiology

Prostate cancer (PCa) is the sixth most common cause of death from cancer in men worldwide and the second most frequently diagnosed cancer in men with a largely increasing incidence in many countries (Jemal et al., 2011). In countries where screening for prostate specific antigen (PSA) is common, the incidence is much higher while the mortality is widely unaffected. However, an increase by 30% of PCa diagnoses each year has been registered in the last 25 years and the incidence is expected to double by the year 2030 (Ruijter et al., 1999). The late age of the PCa patients at diagnosis in combination with a relatively slow tumor growth rate results in the fact that the ultimate death of the vast majority of patients is unrelated to the disease. However, in clinic, prostate tumors show tremendous biological heterogeneity, with some patients dying of metastatic disease within 2 to 3 years of diagnosis (Taylor et al., 2010). This raises the question if an underlying genomic diversity may explain this discrepancy. Recent genomic profiling of human prostate cancer samples by Taylor and colleagues revealed that metastatic tumors harbored the greatest number of chromosomal rearrangements, amplifications, and deletions. The complete loss of chromosome 8p was the most frequent alteration in the prostate oncogenome, detected in up to 50% of cases (Taylor et al., 2010). This chromosomal abnormality is a common event in many epithelial tumors, also described for lung, colon, breast and liver cancer (Bova et al., 1996). Moreover, in nearly half of primary tumors and all examined PCa derived metastases, the phosphoinositide 3-kinase (PI3K) pathway and the androgen receptor (AR) pathway were altered. Additionally, the AR was mutated in all metastatic samples. Therefore, these two famous cancer pathways provide a promising target for therapy in prostate cancer (Taylor et al., 2010).

1.1.2 The androgen signaling cascade & the PI3K pathway

Only testosterone (T) in its free form is able to enter a cell, where it is converted into dihydrotestosterone (DHT) by an enzyme called 5-alpha-reductase (5-alpha R). The AR has a five times higher affinity to bind DHT than T. Binding of androgens to AR leads to dissociation of heat shock protein 90, hyperphosphorylation and translocation to the nucleus where it can up- or downregulate genes under the control of the androgen responsive element (ARE). One of the known target genes is insulin-like growth factor I (IGF-1). AR is essential for growth and differentiation of the normal prostate and is responsible for treatment failure in castration-resistant metastatic disease (Taylor et al., 2010). During endocrine therapy in PCa the levels of T and DHT are reduced by either surgical castration (orchidectomy) or chemical castration (administration of anti-hormones) (Ruijter et al., 1999). Patients show initially an effective response to androgen deprivation therapy, but sooner or later progress from an androgen-sensitive to a castration-resistant phenotype. At this advanced stage treatment is limited to docetaxel chemotherapy (McKeage, 2012). Unexpectedly, it has been shown that AR signaling still plays a critical role in many patients with castration-resistant disease. This can be explained by a hypersensitive AR, an altered AR expression, intracrine synthesis of androgen by the tumor itself or ligand-independent activation by other pathways, such as PI3K/AKT signaling (Figure 1). Phosphoinositide 3-kinases (PI3Ks) are primarily involved in the phosphorylation of membrane inositol lipids. The vast majority of PI3K enzymes are heterodimers comprised of a regulatory and a catalytic subunit (Yuan & Cantley, 2008). They are recruited and activated downstream of receptor tyrosine kinases (RTKs) like the epidermal growth factor receptor (EGFR). The pathway is activated by the binding of growth factors to RTKs which leads to their homo- or hetero-dimerization and self- or cross-phosphorylation. The second messenger, phosphatidylinositol (3-5)-trisphosphate (PIP3) is generated from phosphatidylinositol 4,5-bisphosphate (PIP2) which enables the binding of the nodal kinase AKT, also termed protein kinase B (PKB) with its pleckstrin homology (PH) domain and its activation by two phosphorylation events carried out by

phosphoinositide-dependent kinase 1 (PDK1) and mammalian target of rapamycin complex 2 (mTORC2/PDK2). The tumor suppressor gene PTEN (phosphatase and tensin homolog deleted on chromosome 10) acts as an antagonist of the PI3K/AKT pathway by dephosphorylating PIP3. Activation of AKT/PKB triggers a downstream cascade of further phosphorylation events effecting survival, proliferation, cell cycle progression, growth, migration, and angiogenesis. A well-studied target, which is involved in this pathway, is the serine/threonine kinase mTOR complex 1 (mTORC1) that is a critical regulator of protein synthesis, as well as angiogenesis and cell cycle progression (Sarker et al., 2009).

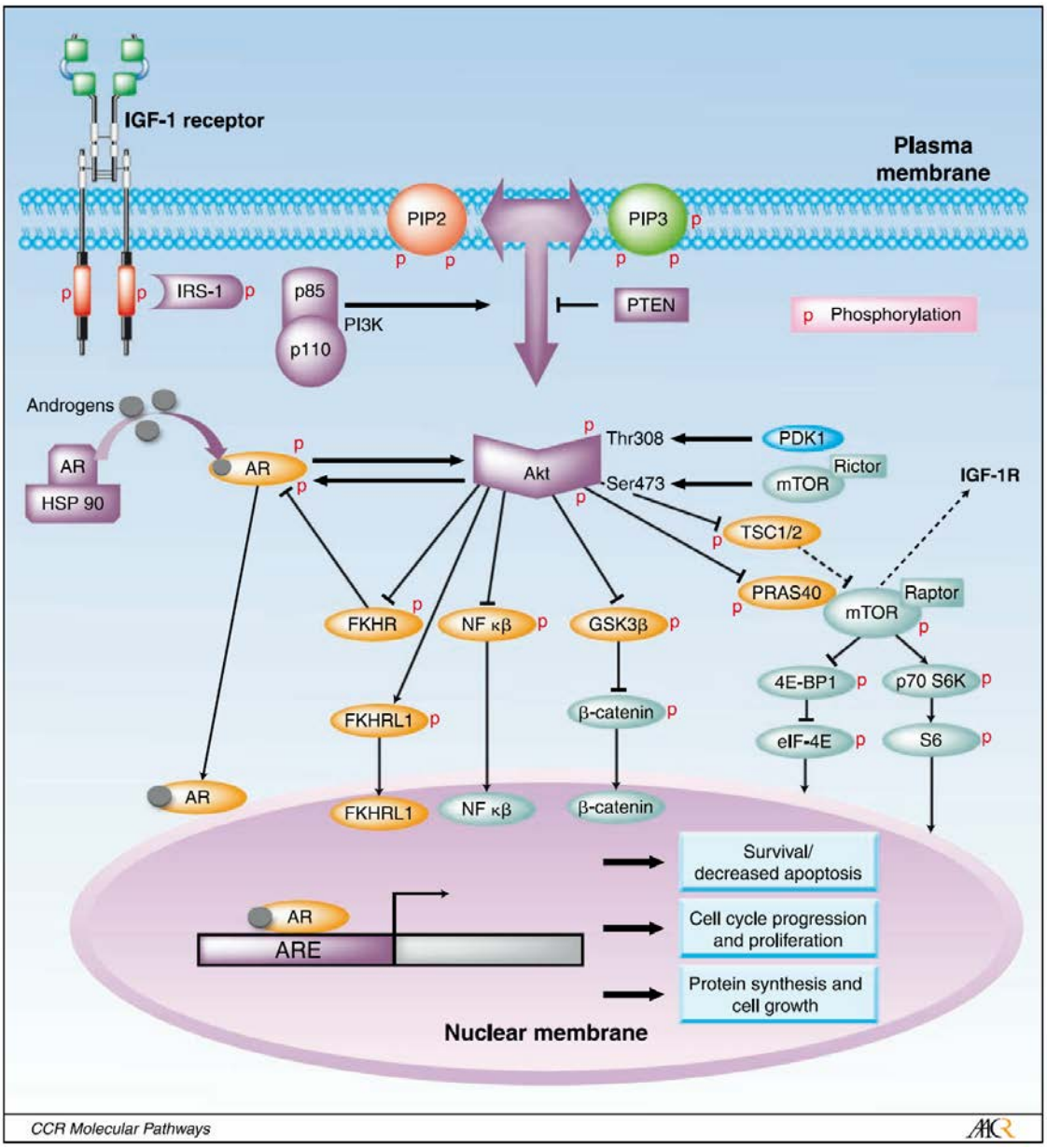

Figure 1: Interaction of the androgen receptor with the PI3K/AKT pathway (Sarker et al., 2009)

1.1.3 Tumor suppressor genes & metastatic suppressor genes

In contrast to oncogenes, tumor suppressor genes (TSGs) are generally considered recessive, which means that both alleles must be inactivated before a cell would be transformed into a cancer cell. Tumor protein 53 (TP53), the most common tumor suppressor gene mutated in almost 50% of all cancers, is one exception for this rule. Because of its tetrameric build-up, one mutant allele is sufficient for the improper function of the vast majority of complexes. Another aspect to be mentioned is the fact that many mutations of the TP53 protein lead to an increased half-life resulting in intranuclear accumulation that would be detected misleadingly as an overexpression. Using the example of another TSG, namely retinoblastoma protein 1 (Rb-1), Knudson was able to show statistically that retinoblastoma is a cancer caused by (at least) two mutational events (Knudson, 1971). The first mutation of a gene appears in a somatic cell or was already inherited from one of the parents by the germline, while the remaining normal allele of that gene will be inactivated by a second hit (Ruijter et al., 1999). Bookstein found an abnormally small mRNA transcript of the Rb-1 gene in the prostate cancer cell line DU145 (Bookstein et al., 1990) which was confirmed by two further studies (Sarkar et al., 1992; Tricoli et al., 1996). DU145 cells lost their tumorigenic ability in nude mice if the normal Rb-1 protein was reconstituted. Aside from being involved in tumor initiation, other genes may suppress the transformation to a metastatic phenotype (Ruijter et al., 1999). The ability to metastasize is one of the hallmarks of cancer cells, defined by Hanahan and Weinberg (Hanahan & Weinberg, 2000, 2011) (Figure 2). For example, E-cadherin, a Ca^{2+} dependent cellular adhesion molecule, is involved in adhesion processes by mediating

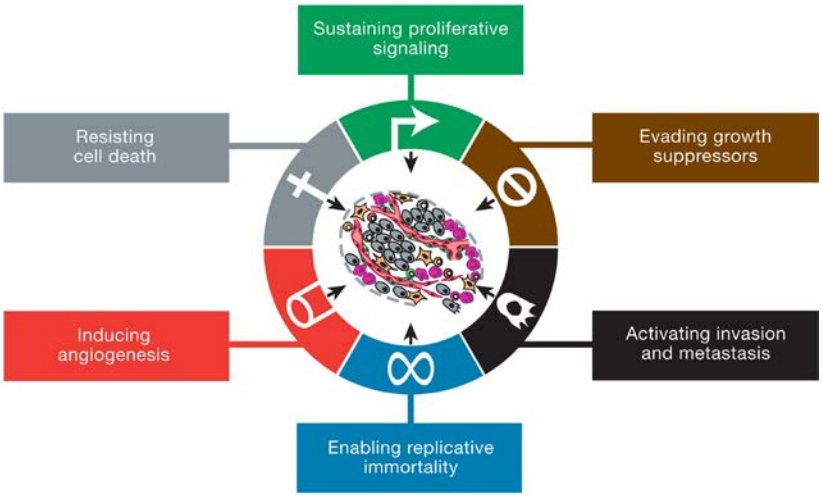

Figure 2: Hallmarks of Cancer (Hanahan & Weinberg, 2011)

epithelial cell-cell recognition. The PCa cell line PC3 is characterized by a homozygous deletion in the α-catenin gene that is essential for E-cadherin function. By introducing an α-catenin expressing vector into these cells, a reversion to a typical epithelial phenotype is induced (Ruijter et al., 1999). PTEN also behaves as a metastatic suppressor gene and its loss of function, through deletion, mutation, or reduced expression, has been well documented in prostate cancer, with varying frequencies (Taylor et al., 2010). Alterations in localized tumors are more often due to copy-number losses, while metastases harbor frequently point mutations. PTEN mutations in patients correlate significantly with poorer prognosis and higher rates of metastasis (Pourmand et al., 2007).

1.1.4 Risk factors

While the lowest risk developing PCa can be found in men from Asian populations, the highest risk lies in black Caribbean and black African men, suggesting genetic determinants as major risk factors. Familial clustering could be clearly demonstrated in several twin studies and studies comparing close relatives. A rare autosomal dominant susceptibility gene, which predisposes to cancer development if inherited, could explain the significant increase observed in brothers and fathers of PCa patients. Beside an inherited component other observations have been made to explain especially racial and ethnic differences in PCa incidence (Ruijter et al., 1999). Wu reported a DHT-to-T ratio corresponding to the respective risk of developing PCa in African-Americans, Caucasian-Americans and Asian-Americans (Wu et al., 1995). Similarly, Ross demonstrated that young Japanese men have the lowest 5-alphaR activity in this group (R. K. Ross et al., 1992). They already showed previously that young African-American males have a 15% higher serum T-level compared to their white counterparts (R. Ross et al., 1986). Schwartz and Hulka were the first who hypothesized a protective effect of the secosteroid vitamin D against developing PCa (Schwartz & Hulka, 1990). In fact, elderly as well as black men have in general lower levels of vitamin D and at the same time an increased incidence. Additionally, migrant Asians who adopted Western diet, which widely lacks in large amount of vitamin D-rich fish oil, exhibit an increased incidence (Ruijter et al., 1999).

1.2 The Endoplasmic Reticulum

The endoplasmic reticulum (ER) is structurally highly dynamic and can be considered as a multifunctional organelle with main functions in protein synthesis and processing as well as maintaining the Ca2+ homeostasis inside the cell (Berridge, 2002). It forms a membranous network out of tubules and cisternae spread throughout the cell. Depending on the function to be fulfilled, the ER adopts different morphologies distinguishable into the nuclear envelope (NE), the smooth ER (sER), and the rough ER (rER). The latter is associated with a broad number of ribosomes involved in protein synthesis (Baumann & Walz, 2001). Proteins destined for secretion or exposure on the cell surface, are co-translationally translocated into the lumen of the ER where they are properly folded and delivered via the secretory pathway to their desired destination. In contrast, the sER serves as the main calcium storage of the cell, regulating the in- and efflux of Ca2+ from the cytoplasm. In addition, the biosynthesis of steroids, cholesterol and phospholipids takes place at this site of the ER (Tsai & Weissman, 2010). Nevertheless, a high calcium level is also essential for protein folding and the function of several Ca^{2+} dependent chaperones (Berridge, 2002). The ER harbors many chaperones and lectins like the glucose-regulated proteins (GRPs), calnexin (CNX), calreticulin (CRT), peptidyl-prolyl isomerases (PPI), and protein-disulphide isomerase (PDI), which catalyzes the formation of disulfide bonds. Beside to assist protein folding they are also involved in a complex quality control system which ensures that only properly folded proteins will leave the ER. Unfolded glycoproteins with accessible N-linked monoglucosylated regions serve as binding sites for the lectin-like chaperones CNX and CRT. Just the removal of the last glucose destroys this binding site and allows the proteins to exit the ER. Another mechanism is based on hydrophobic regions which are recognized by the glucose-regulated chaperone GRP78/binding immunoglobulin protein (BiP). Recently it has been shown that some GRP78 bound proteins are designated as misfolded, which mediates their degradation by the ER-associated degradation (ERAD) pathway and their retrograde translocation to the cytoplasm (Boelens et al., 2007).

1.2.1 ER stress & the unfolded protein response

Several ER stress conditions including hypoxia, glucose deprivation, oxidative stress, viral infection, high fat or cholesterol, altered glycosylation, and mutations in specific proteins can cause accumulation and aggregation of unfolded or misfolded proteins in the ER and activate the unfolded protein response (UPR) (Tsai & Weissman, 2010). Stress response is mediated through three ER stress sensors located at the membrane of the ER (Figure 3). These receptors are activating transcription factor 6 (ATF6), inositol-requiring enzyme 1 (IRE1), which are both mediating transcriptional regulation, and protein kinase-like ER kinase (PERK), which represses global protein synthesis (Boelens et al., 2007). Under normal conditions these transmembrane proteins are maintained inactive by the association with GRP78, an ER chaperone. If unfolded proteins accumulate, GRP78 dissociates and binds to them which leads to receptor activation. The PERK pathway is the first one getting active by dimerization and cross-phosphorylation. Active PERK phosphorylates the alpha subunit of eukaryotic translation initiation factor 2 (eIF2α), which initiates inhibition of protein translation and promotes preferential translation of transcription factor ATF4 (Lin & Popko, 2009). After the release of GRP78 from ATF6, its transport to the Golgi apparatus is permitted, where it is cleaved by resident proteases, SP1 and SP2, to become an active transcription factor (p50ATF6). Active p50ATF6 shuttles to the nucleus and induces the expression of genes harboring ER stress response elements (ERSE), including mainly chaperone proteins as well as X box-binding protein 1 (XBP1). IRE1 is thought to be the last activated arm during UPR. After dimerization and auto-phosphorylation, the endoribonuclease activity of active IRE1 induces alternative splicing of XBP-1, whose expression was previously induced by ATF6. The splice variant (sXBP1), lacking a 26-nucleotide intron, encodes a transcription factor which targets genes, such as ER chaperones and heat shock proteins. Additionally to this pro-survival effect, it also recruits the adaptor molecule TNF-receptor-associated factor 2 (TRAF2) which results in apoptotic cell death (Szegezdi et al., 2006).

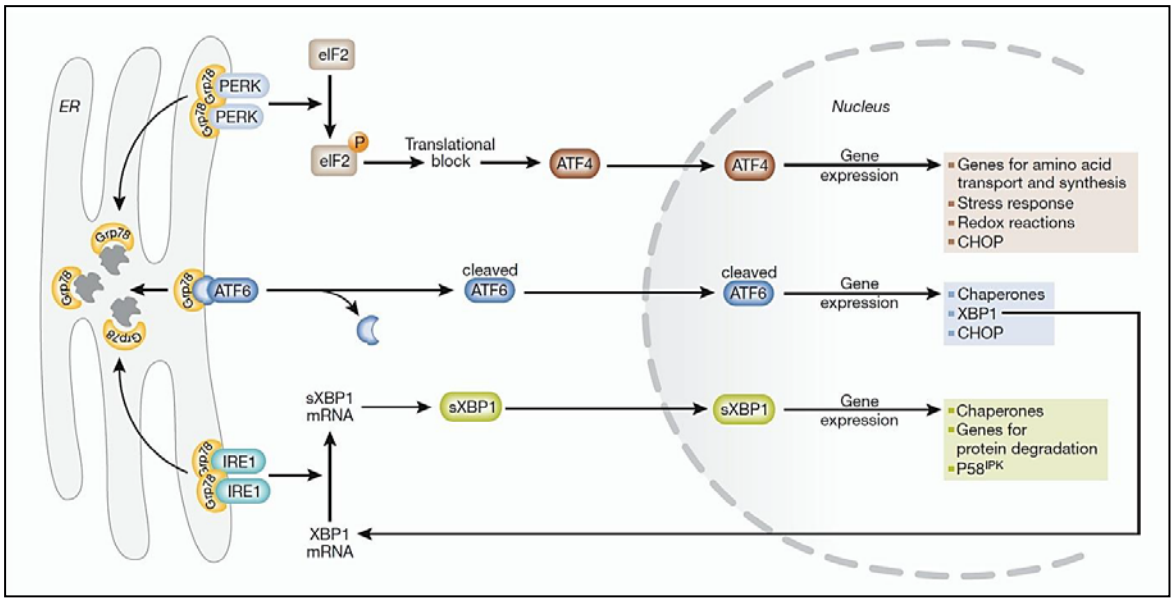

Figure 3: ER stress response (Szegezdi et al., 2006)

1.2.2 ER mediated apoptosis

If restoration of normal ER function fails and ER stress is prolonged, programmed cell death (apoptosis) ensues. The transcription factor C/EBP homologous protein (CHOP) is downstream of the PERK-eIF2α-ATF4 pathway and promotes apoptosis by inducing either gene expression of growth arrest and DNA damage-inducible protein 34 (GADD34), endoplasmic reticulum oxidoreductin 1 (ERO1α) and Tribbles-related protein 3 (TRP3) or downregulation of anti-apoptotic protein B-cell lymphoma 2 (BCL2). GADD34 is interacting with protein phosphatase 1 (PP1) which can dephosphorylate eIF2α and thus release the translational block. It is thought that then pro-apoptotic proteins are synthesized. Similarly, the repression of BCL2 by CHOP increases the proportion of pro-apoptotic proteins. Furthermore, CHOP up-regulates DR5, a member of the death receptor family. c-Jun N-terminal kinase (JNK) is activated by the IRE1-TRAF2-ASK1 pathway and phosphorylates BCL2 which suppresses its anti-apoptotic activity. But JNK also phosphorylates pro-apoptotic members of the BCL2 family which enhances their potential. Induction of apoptosis by CHOP overexpression is associated with the activation and mitochondrial translocation of Bcl-2-associated X protein (Bax) (Szegezdi et al., 2006). Studies by Du and colleagues have indicated that TRB3 can bind to the pro-survival serine/threonine kinase Akt, thereby preventing its phosphorylation, and promote apoptosis (Du et al.,

2003). CHOP activity is increased by post-translational phosphorylation through the mitogen-activated protein kinase (MAPK) p38. All the upstream targets lead finally to the activation of caspases resulting in a cleavage cascade. In rodents, caspase 12 has been identified as an initiation caspase localized at the ER. Nevertheless, neither a definitive substrate nor a human orthologue have been identified yet (Hermel & Klapstein, 2011; Szegezdi et al., 2006).

1.2.3 ER stress in cancer

Many studies focused on the role of ER stress and its implication in the pathophysiology of several neurodegenerative and cardiovascular diseases (Szegezdi et al., 2006). More and more evidence indicates an important role of the unfolded protein response (UPR) in diseases such as diabetes mellitus, liver diseases and inflammatory disorders (Lin & Popko, 2009). Cancer cells in a rapidly growing tumor face a harsh microenvironment, including hypoxia, nutrient deprivation and acidosis, which all might induce ER stress by acting as an environmental sensor. An altered expression of many ER stress-related genes and their corresponding proteins has been observed in various cancers. Expression of GRP78/BiP and GRP94, both ER chaperones, is increased in at least 10 different cancers, such as lung, breast, colon cancer, and hepatocellular carcinoma (HCC). In the latter cancer type, also the lectin-like chaperone calreticulin is overexpressed and can be detected in the serum of these patients in form of autoantibodies or because of the development of protein fragments. Additionally, in breast cancer, calnexin is up-regulated which correlates with enhanced resistance to ER stress (Moenner et al., 2007). Under hypoxic conditions, UPR plays an important role in cancer cell survival. It has been shown in xenograft models that the IRE1-XBP1 axis promotes tumor growth. IRE1 signaling is enhanced by the protein tyrosine phosphatase 1B, which is also involved in human breast cancer (Gu et al., 2004). Additionally, under ER stress IRE1 leads to ERK1 activation (Nguyen et al., 2004). Unconventional splicing of XBP-1 has been described in cancers, such as HCC. Loss of XBP1 further leads to enhanced ROS generation which sensitizes cells to death from oxidative stress. The different levels

of XBP1 in tumors correlate with their growth rate, as well as inversely with glucose availability, suggesting a response to glucose starvation. Also PERK is essential for tolerating hypoxia during tumor cell development. Tumor cells lacking PERK are showing reduced viability in hypoxia. Furthermore, it was found that PERK interacts with the oncogenic protein NCK as part of its regulatory mechanisms (Kebache et al., 2004). A role of UPR during angiogenesis and dormancy has been suggested recently. ATF6 has been shown to be essential for long-term survival of dormant cells and resistance to chemotherapy. ATF6 activation increases the expression of Rheb which activates mTOR signaling independently of AKT. The mRNA level of ATF6 and the amount of translocated protein to the nucleus is increased in HCC compared to noncancerous liver tissues (Tsai & Weissman, 2010). During ER stress VEGF, a pro-angiogenic glycoprotein, is upregulated. The inhibition of cyclin D1, downstream of PERK, contributes to tumor dormancy by cell cycle arrest in G1 phase (Boelens et al., 2007). Conversely, knockdown of PERK in human breast cancer cells leads to an arrest in G2/M phase. This is explained by reduced activity of Nrf2, a transcription factor of antioxidant response elements and an accumulation of ROS and oxidative DNA damage resulting in activation of DNA double strand-break checkpoint (Tsai & Weissman, 2010). Meanwhile, targeting ER-dependent pathways found its way into anticancer therapy by the recent discovery that treatment of human leukemia cells with sorafenib induces apoptosis by mediating ER stress (Rahmani et al., 2007).

1.2.4 PI3K and metabolism

Signal transduction is known to regulate nutrient metabolism. In cancer cells, oncogenes drive the uptake of nutrients through activated signaling pathways. But also the reciprocal way, the modulation of signaling and transcriptional networks by protein modifications becomes more and more accepted. Glycosylation is such nutrient-sensitive protein modification that has been shown to modulate signaling, gene expression and metabolism. 3 to 5% of the glucose taken up branches off glycolysis and is thought to be processed by the hexosamine pathway to UDP-N-acetylglucosamine (UDP-GlcNAc).

UDP-GlcNAc is used to initiate N-glycosylation by the transfer of GlcNAc-phosphate onto the lipid dolichol-phosphate. It is also used in the Golgi apparatus for remodeling N-glycans to generate tri-antennary and tetra-antennary structures, which are important for the regulation of receptor surface expression. Glucose deprivation has an effect on the surface expression of growth factor receptors, which are common targets of N-glycosylation. It also directly affects the surface expression of nutrient transporters, such as glucose transporter type-2 (GLUT2). At the same time, activation of the PI3K/AKT pathway is known to increase the uptake of glucose and the level of GlcNAc-branched glycans at the cell surface (Wellen & Thompson, 2012). Under PTEN loss, AKT activation stimulates the expression of ectonucleoside triphosphate diphosphohydrolase 5 (ENTPD5), an ER-resident UDPase with a crucial role in N-glycosylation, possibly due to the activation of an unknown downstream transcription factor. Expression levels of growth factor receptors were reduced in the absence of ENTPD5, most likely due to hypoglycosylation (Fang et al., 2010). These findings together suggest a positive feedback-loop among PI3K/AKT signaling, glucose uptake, gene expression and metabolism (Figure 4).

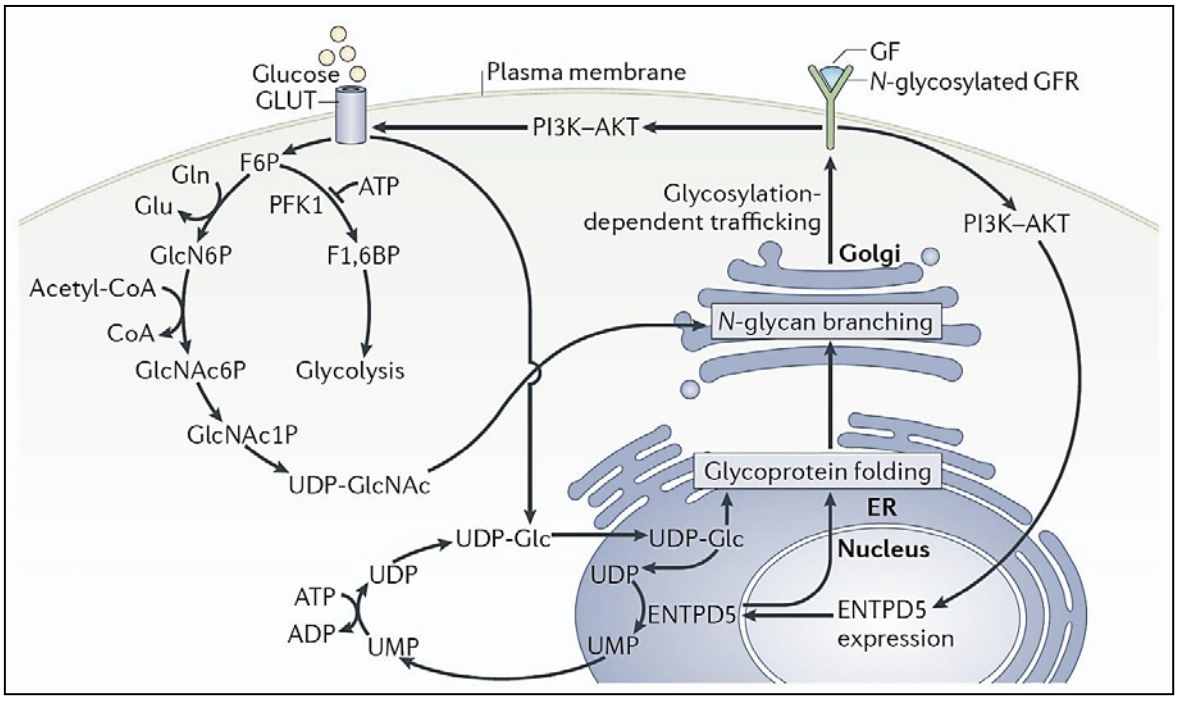

Figure 4: Linkage of glycosylation and metabolism (Wellen & Thompson, 2012)

1.3 Glycosylation

Glycosylation, the addition of sugar molecules to amino acids, is one of the most frequent co- and post-translational protein modifications, which is highly conserved in almost all eukaryotes. Glycosylation of proteins can enhance solubility, improve folding, facilitate secretion, modulate antigenicity and increase *in vivo* half-life by protecting from proteases (Csala et al., 2012). Central to the biosynthesis of glycoproteins are highly specific enzymes called glycosyltransferases, which are classified on the basis of the sugar they transfer (e.g., galactosyltransferases and sialyltransferases) and the linkage they form (e.g., α2,6 sialyltransferases). Depending on the glycosidic bond formed the process can be further divided into two classes: oligosaccharides linked to the amidic nitrogen of asparagine (N-linked) and those linked to an oxydril side group of serine or threonine (O-linked). While O-glycosylation occurs primarily in the Golgi apparatus, N-glycosylation is initiated exclusively in the ER (Dall'olio, 1996). In contrast to O-glycosylation, N-glycosylation targets proteins in their unfolded state. The translocation of proteins into the ER occurs through a peptide channel composed of Sec61αβγ subunits. This transmembrane channel forms an aqueous pore whose conformation changes by ribosome binding, leading to the opening of the channel and allowing proteins to get translocated into the lumen of the ER (Csala et al., 2012).

1.3.1 N-glycosylation

Substrate specific glycosyltransferases build in a sequential process a high-mannose oligosaccharide onto a lipid linked pyrophosphate carrier. These enzymes need as substrates activated monosaccharides, nucleotide sugars (e.g., UDP-glucose). The first two GlcNAc and five mannose molecules are built up on the cytosolic side of the ER membrane (Csala et al., 2012). The intermediate generated ($Man_5GlcNAc_2$-PP-Dol) is translocated across the membrane into the lumen of the ER, a process dependent on the flippase Rtf1 (Kelleher & Gilmore, 2006). Here, the biosynthesis continues by the addition of four more mannose and three glucose molecules (Csala et al., 2012). The core N-glycan is then transferred en bloc from the isoprenoid lipid carrier to selected asparagine

residues within the consensus sequence asparagine-X-serine/threonine of nascent polypeptides (where X can be any amino acid expect proline) (Mohorko et al., 2011). This step is carried out by the heteromeric enzyme oligosaccharyltransferase (OST) (Figure 5). An aging phenomenon is the aspect that not all potential acceptor sites which enter the ER lumen are effectively used or are instead used with low efficiency *in vivo*. Estimations state approximately 35% of consensus glycosylation sites which are not modified *in vivo*. Transmembrane spans, prolines and disulfide bonds near the consensus sequence are reducing N-glycosylation efficiency at this site. In addition, N-glycosylation occurs less frequently near the C-terminus of proteins. Furthermore, it has been shown that N-X-T serves as a better substrate than N-X-S and that in humans even N-X-C is recognized in one case (Kelleher & Gilmore, 2006).The fully assembled tetradecasaccharide ($Glc_3Man_9GlcNAc_2$) can be trimmed by specific glycosidases and further modified in the Golgi apparatus to a more complex structure (Dall'olio, 1996).

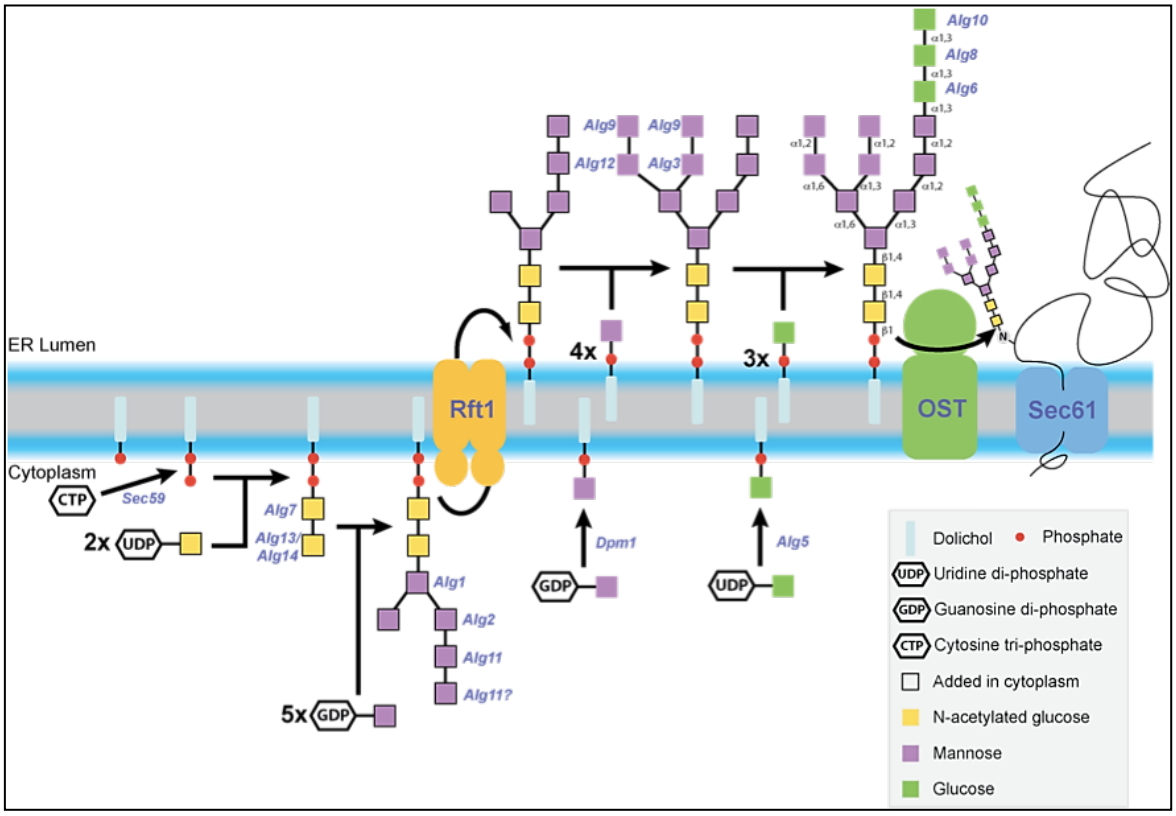

Figure 5: The process of N-glycosylation (Clemons Lab, California Institute of Technology, accessed January 28, 2013, http://clemonslab.caltech.edu/n-linked-glycosylation.html)

1.3.2 Mammalian oligosaccharyltransferase

The mammalian oligosaccharyltransferase is a multiprotein complex composed of seven subunits and exists in at least four different variants (Schulz & Aebi, 2009) (Figure 6). It is integrated in the membrane of the ER, catalyzing the en bloc transfer of a preassembled oligosaccharide to the side-chain amide group nitrogen of an asparagine residue contained in a specific amino acid sequon of the polypeptide substrate (Mohorko et al., 2011). In Archaea, several cell surface glycoproteins and flagellins are modified with tetrasaccharides. The sequence motif to be glycosylated matches the sequon in eukaryotic organisms. Interestingly, also here a dolichol-pyrophosphate-linked oligodaccharide is used as a donor. In eubacteria, a single protein, namely PglB, catalyzes N-linked glycosylation of several cell surface proteins. PglB is homologous to the STT3 subunit of the eukaryotic OST. Furthermore, only the Stt3 protein has archae-bacterial homologues. The final evidence, demonstrating Stt3 as the catalytic subunit, came from reconstitutional studies in E.coli. Stt3 is the largest and most conserved polypeptide of OST and appears in two different isoforms, with either Stt3-A or Stt3-B being incorporated into the mammalian complex. Both human variants share 59% amino acid sequence identity, but they differ in their acceptor substrate selectivity. While Stt3-A is more selective, Stt3-B is 8- to 12-fold more active, but in consequence shows a reduced selectivity. Stt3-B was found to act preferentially posttranslationally, whereas

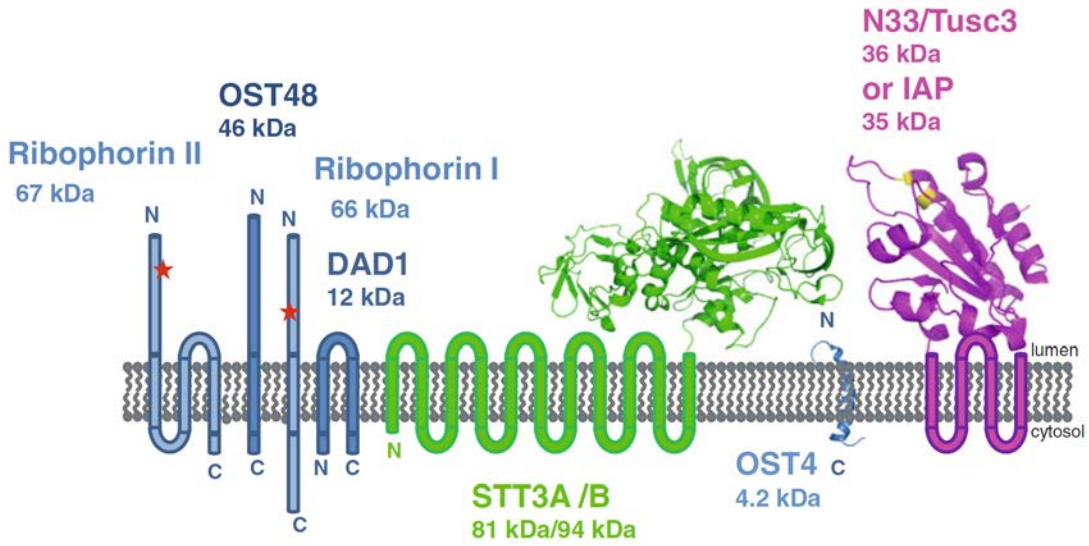

Figure 6: The human oligosaccharyltransferase (OST) complex (Mohorko et al., 2011)

Stt3-A catalyzes cotranslational glycosylation. The absence of both subunits leads to hypoglycosylation and decreased levels of ribophorin I. Ribophorin I appears in about equal amounts relative to membrane-bound ribosomes, suggesting a physical interaction which has been confirmed by cross-linking experiments. Interestingly, ribophorin II is upregulated in drug-resistant human breast cancer cells and downregulation can restore docetaxel-induced apoptosis in these cells. Downregulation of ribophorin II leads to hypoglycosylation of P-glycoprotein, which is a key player in conferring drug resistance and its complete glycosylation is sufficient for functional activity and stable membrane integration. The ribophorins provide binding sites for translating ribosomes, but are not essential for glycosylation of secretory and multi-spanning membrane proteins; however, single-spanning membrane proteins require their expression for efficient glycosylation. OST48 is an essential subunit that possibly links ribophorin I with ribophorin II in the active OST complex. OST48 was also shown to interact with DAD1, which was first described as defender against apoptotic cell death. DAD1 instability results in severe hypoglycosylation that might induce apoptosis by preventing structural and functional integrity of the OST complex. At least, degradation of the mutated DAD1 protein at nonpermissive temperatures induces apoptosis. Very little is known about the OST4 subunit comprising a single transmembrane helix with a very short luminal segment. The yeast homolog Ost4p seems to regulate the incorporation of OST3p and OST6p and single-point mutations also disrupt the interaction between OST3p with Stt3p (Mohorko et al., 2011).

1.3.2.1 Tumor suppressor candidate 3 (TUSC3)

The two paralogues, N33/TUSC3 and IAP/MagT1 are mutual exclusive subunits of the mammalian OST. They share 70% sequence identity with each other and 20% sequence similarity with the yeast OST subunits Ost3p and Ost6p, respectively (Knauer & Lehle, 1999). The two paralogues in yeast possess different protein substrate specificity at the level of individual glycosylation sites (Jamaluddin et al., 2011). The OST3-complex is much more abundant, about 3 up to 4-fold higher, than the OST6 complex (Schwarz et al., 2005). Ost3p is neither essential for the assembly or stability of the OST complex nor

lethal for yeast, but disruption causes hypoglycosylation of proteins *in vivo* and a 2-fold reduction of OST activity *in vitro*. Reduction in oligosacharide transfer affected some but not all acceptors (Karaoglu et al., 1997). Jamaluddin proposed a model, where Ost3p and Ost6p are increasing glycosylation efficiency by transiently binding stretches of nascent polypeptides to inhibit their folding and prolong the time they are accessible to the OST active site (Jamaluddin et al., 2011). Schulz and colleagues showed previously that the increased efficiency of glycosylation is a result of the oxidoreductase and redox-dependent peptide binding activities of Ost3p/Ostp6 (Schulz & Aebi, 2009). N33/TUSC3 exists in two splicing variants, differing from each other only in the last five amino acids. Only N33-1 co-sediments with the active OST complex, for which reason it is thought that N33-2 and IAP/MagT1 are just weakly associated. Protein domain prediction suggests a thioredoxin-like fold with a characteristic CxxC active-site motif, which is essential for oxidoreductase activity (Figure 7). Proteins with this domain commonly harbor disulfide oxidoreductase activity, required specifically in oxidative protein folding. Disulfide oxidation and N-glycosylation are linked processes, because disulfide bond formation can compete with glycosylation in specific substrates (Schulz et al., 2009). The four predicted membrane-spanning segments of N33/TUSC3 integrate this OST subunit into the membrane of the ER (Mohorko et al., 2011). Zhou and colleagues suggest N33/TUSC3 and IAP/MagT1 as magnesium transporters, disregarding their homology to the yeast OST subunits (Zhou & Clapham, 2009). Deficiencies of human N33/TUSC3 result in isolated cognitive defects and mental retardation (Garshasbi et al., 2008; 2011)

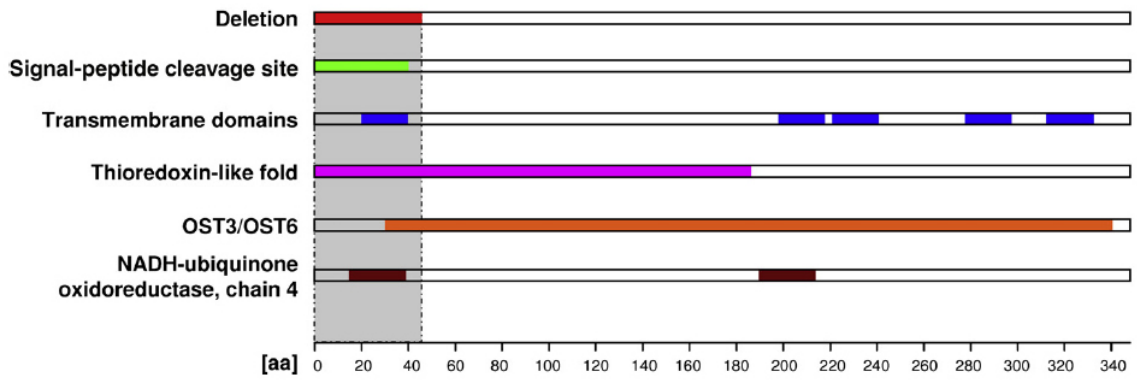

Figure 7: Predicted functional domains of TUSC3 (Garshasbi et al., 2008)

1.3.2.2 TUSC3 in ovarian cancer

Allelic imbalance at regions of chromosomal arm 8p is documented frequently in ovarian tumors by several studies. Systematic screening of region 8p22 by using publicly available gene profiling data could narrow down the list of all 22 genes localized there to 8 putative tumor suppressor genes (Pils et al., 2005). By expression analysis this list could be further reduced to 5 potential candidates with 2 of them, one being TUSC3, formerly called N33, carrying out a noteworthy function. Pils and colleagues observed a grade-dependent expression of TUSC3 in the ovarian cancer samples examined. Tumors which were classified into tumor grade 3, representing a predominantly solid subtype, showed a significantly lower expression of TUSC3 compared with tumors of grade 1 or 2, and epithelial-enriched normal tissues. When correlated to the International Federation of Gynecology and Obstetrics (FIGO) classifications, the expression pattern changed between FIGO stages I-II, while FIGO stages beyond II are characterized by the occurrence of (micro)-metastases. Loss of expression of TUSC3 in patients had a significant impact on overall survival, especially in combination with the down regulation of ADP-ribosylation factor guanine nucleotide exchange factor 6 (EFA6R), another putative TSG located at 8p22. This apparent impact on survival was, however, independent from tumor grade. In addition, a complete loss of EFA6R expression was also observed in several ovarian cancer cell lines. Reconstitution of TUSC3 in two cell lines lacking its expression led to a decrease in cellular proliferation *in vitro* and cellular adhesion to collagen I, an extracellular matrix component. In a later study, promoter hypermethylation was proposed as an epigenetic mechanism for silencing gene expression of TUSC3 (Pils et al., 2012). Methylation studies revealed a significant correlation of TUSC3 expression and methylation in cancer cell lines as well as tumor samples. TUSC3 promoter hypermethylation was observed in almost a third (29.4%) of patient samples. Patients with methylated TUSC3 promoter had significantly shorter progression-free and overall survival rates (Figure 8).

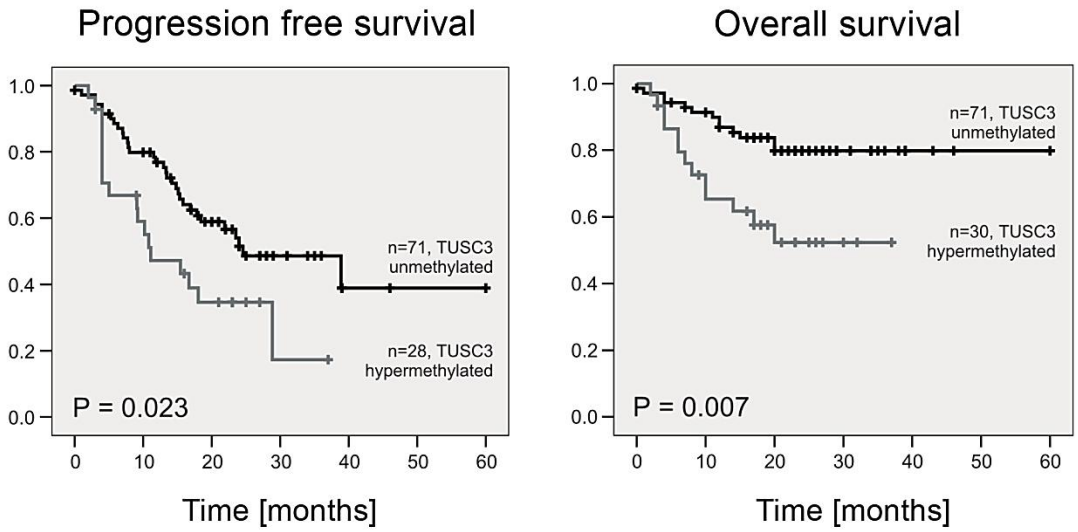

Figure 8: Kaplan-Meier survival curves for tumor samples from patients with hypermethylated or unmethylated TUSC3 promotor region (Pils et al., 2012)

1.3.3 N-glycosylation in cancer

For over 45 years the occurrence of aberrant glycosylation has been observed in essentially all types of experimental and human cancers, and many tumor-associated antigens turned out to recognize glycosyl epitopes. Nevertheless, the question still remains, whether this is a result or a cause of cancer (Hakomori, 2002). The expression of highly branched and heavily sialylated glycans or of incomplete forms are most frequently described cancer related changes of glycosylation and the result of an altered regulation of one or more key glycosyltransferases. Altered glycosylation in cancer biology has been studied by two approaches: 1) the modification of glycosylation patterns by means of glycosylation inhibitors or glycosidase treatments and 2) selection of subpopulations of cancer cells for increased or reduced metastatic ability or resistance to a given lectin (Dall'olio, 1996). A more invasive and metastatic phenotype provides a selective advantage for tumor cells during progression (Janik et al., 2010). The following known examples of the impact of glycosylation on cancer should emphasize its significance. Treatment of murine and human colon cancer cell lines with KI-8110, a specific sialyltransferase inhibitor, leads to a dramatic reduction of lung and liver metastasis formation. Tunicamycin inhibits the transfer of N-acetlyglucosamine-1-phosphate to dolichol monophosphate, which is the first step of N-glycosylation, eventually resulting in

proteins without N-linked chains. Castanospermine inhibits glucosidase I, the first "trimming" enzyme, giving rise to high mannose structures. Treatment with these agents leads to a dramatic reduction of pulmonary metastases in murine melanoma cells. The same effect could be observed in mouse mammary tumor cells after treatment with tunicamycin alone. However, the narrow window efficacy of tunicamycin eliminates its potential as a therapeutic agent in patients (Morin & Bernacki, 1983). Clones of mouse melanoma cells resistant to wheat germ agglutinin (WGA) display a dramatic reduction in metastatic ability. These cell clones showed a reduced expression of surface sialic acid and, therefore, increased binding to collagen type IV and fibronectin. About 90% of colon cancer specimens showed increased activity of an enzyme catalyzing the formation of α2,6-linked sialic acid which is recognized specifically by the Sambucus nigra lectin (SNA). Phytohemagglutinin (PHA-L) is a lectin recognizing β1,6 branching of N-linked chains, whose increased surface expression has been directly associated with a metastatic potential and is one of the most important cancer related changes. Increased affinity to PHA-L could be detected in all breast carcinomas and epithelial hyperplasia compared with fibroadenomas and hyperplasia without atypia (Dall'olio, 1996).

1.3.4 Selected targets of N-glycosylation

Receptor tyrosine kinases (RTK) are transmembrane glycoproteins and their activation results in widely pro-proliferative and anti-apoptotic signals. N-linked glycosylation is crucial for the maturation of these receptors, including insulin growth factor receptor (IGFR), vascular endothelial growth factor receptor (VEGFR), and the RTK family. Inhibition of N-linked glycosylation has been shown to reduce protein levels of IGFR and prevent ligand binding and thus activation of EGFR. Moreover, it has been shown that the activity of EGFR is regulated by specific glycosylation side chain modifications which are even required for signaling. It could be further shown that the protein level of four RTKs is decreased after treatment with N-linked glycosylation inhibitor, tunicamycin. This could be explained by the retention of the receptor in the ER or Golgi and displays a promising treatment option in cancer therapy (Contessa et al., 2008). During metastasis, the main

cause of cancer deaths, some tumor cells acquire the ability to migrate out of the primary tumor and form a secondary tumor in a distant organ. Integrins, a major family of cell-cell and cell-extracellular matrix (ECM) adhesion proteins, are up-regulated in these migratory cells. There are about 24 distinct integrin molecules differing in their non-covalently linked α and β subunits and their substrate specificity, but in general, the most prevalent peptide sequence recognized is comprised of arginine-glycin-aspartic acid (RGD), a motif found in many ECM proteins, such as fibronectin, collagens and vitronectin. All integrins contain over 20 potential glycosylation sites and evidence has been obtained that glycosylation regulates their function. Glycosylation appears to be important for both, structure and function. Integrin dimers require conformational changes to become active. The ability to form functional dimers depends on the presence of N-linked oligosaccharides (Janik et al., 2010). E-cadherin is a type-I cadherin that mediates specific cell-cell adhesion in a calcium-dependent manner. It is comprised of a single transmembrane domain, a cytosolic domain and five ectodomains. The first extracellular domain mediates weak binding to an opposing cadherin. Stronger cell-cell adhesion occurs during lateral clustering of cadherins and the involvement of catenins which interact with their cytoplasmic domains. β-catenin and γ-catenin (plakoglobin) also link the cadherin to the cytoskeleton through interaction with α-catenin. This complex of cadherin with catenin is required for normal cell-cell adhesion and alteration can result in tissue disorders, cellular de-differentiation and invasiveness of tumor cells. In many human carcinomas neither mutations nor epigenetic or transcriptional silencing of its gene (CDH1) could be detected to explain its dysfunction, which suggests mechanisms operating at the post-translational level. E-cadherin has four possible sites for N-glycosylation, localized in its extracellular domain (EC4 and EC5). It has been shown by Zhao et al. that N-glycans at Asn633 are essential for folding, trafficking, and its proper expression (Zhao et al., 2008). Furthermore, glycosylation influences the stability of adherens-junctions. E-cadherin of a canine mammary tumor cell line shows an increase in sialyation, β1,6 branched N-glycan structures and the presence of a few high mannose structures (Pinho et al., 2011).

1.4 Aim of this thesis

Loss of the short arm of chromosome eight (8p) is a common event in prostate carcinogenesis (Figure 9). Especially chromosomal band 8p22, harboring TUSC3 (N33) and only 21 other genes, is frequently affected (Bova et al., 1996). Bova et al. were the first who identified TUSC3 as a tumor suppressor candidate gene in metastatic prostate cancer and later homozygous loss was also detected in the pancreatic cancer cell line MiaPaCa-2 (Bashyam et al., 2005). Frequently, homozygous deletions in tumors are indicators for regions harboring tumor suppressor genes. In a previous study, our group investigated the role of TUS3 in ovarian cancer and demonstrated clinical relevance as a predictive factor for patient outcome. Another study showed aberrant methylation of TUSC3 also in prostate cancer tissues (Kekeeva et al., 2007). This data goes along with our own observation of the methylation status in patients diagnosed with prostate cancer (Pils et al., 2013). Taken together, these observations suggest a possible role of silencing TUSC3 in prostate cancer and an influence on cancer progression in that tumor entity. Though, only little is known about the molecular function of TUSC3. In the first part of this thesis, the influence of TUSC3 downregulation on prostate cancer cell behavior is studied, while the second part explores the basis for these observations. The aim of this thesis was to unravel the molecular function of TUSC3 in prostate cancer cells and to find an explanation for its putative role in tumor formation and progression.

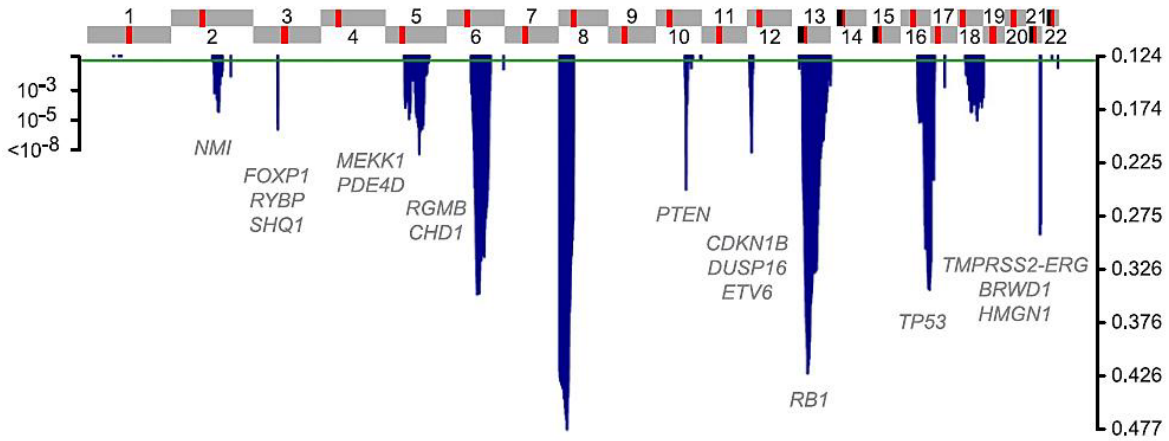

Figure 9: Frequencies of deleted chromosomal regions in prostate cancer (Taylor et al., 2010)

2 Materials and Methods

2.1 Cell culture techniques

2.1.1 Media, buffers and reagents

10xPBS (1.37M NaCl, 14.7mM KH_2PO_4, 78.1mM Na_2HPO_4, 26.8mM KCl); 10xTrypsin/EDTA (PAA, L11-003); Crystal Violet (Sigma-Aldrich, C6158); Dimethyl sulfoxide (DMSO) (Sigma Aldrich, D2438); DMEM, High Glucose, GlutaMAX, Pyruvate (GIBCO, 31966-021); Fetal Bovine Serum (FBS), Standard Quality, Heat Inactivated (PAA, A15-104); G 418 disulfate salt powder (Sigma Aldrich, A1720); Lapatinib and Erlotinib, kindly provided by Thomas Grunt (Medical University of Vienna, Austria); Mitomycin c (Sigma Aldrich, M4287); PBS/EDTA (1xPBS/1.35mM EDTA); Penicillin-Streptomycin, Liquid (GIBCO, 15070-063); Polyprene (Santa Cruz, sc-134220); Puromycin (PAA, P11-019); RPMI 1640 Medium, GlutaMAX (GIBCO, 61870-010).

2.1.1 Cell lines

Human prostate cancer cell lines DU145 and PC3 were received from laboratories of Karel Soucek (Institute of Biophysics, Academy of Science of the Czech Republic, Brno, Czech Republic) and cultured in RPMI Media 1640 supplemented with 10% FBS and 100µg/ml Penicillin-Streptomycin. Transduced cells were maintained in medium containing puromycin (1.5µg/ml). Human embryonic kidney 293 (HEK293) cells were obtained from laboratories of Peter Petzlbauer (Department of Dermatology, Medical University of Vienna, Austria) and cultured in DMEM supplemented as RPMI.

2.1.2 Cell line maintenance

Cells were passaged before forming a monolayer. For this purpose, the medium was soaked off and the plate was washed once with 1ml 1xPBS/EDTA (100mm dish) or 500µl 1xPBS/EDTA (60mm dish), respectively, followed by the addition of 1ml 1xTrypsin/EDTA per 100mm dish or 500µl per 60mm dish. The plate was incubated for 5 minutes at 37°C in a humidified incubator with 5% CO_2. To inhibit Trypsin, 4ml complete medium was

added to a 100mm dish or 2.5ml to a 60mm dish, respectively. Cells were resuspended by pipetting several times up and down until no cell clumps were visible and an appropriate volume of splitted cells (e.g. 0.5ml for 1:10 or 1ml for 1:5) was put back onto the plate. Medium was added to a final volume of 10ml (100mm dish) or 3ml (60mm dish) and the plate was placed back into a humidified incubator.

2.1.3 Counting cells

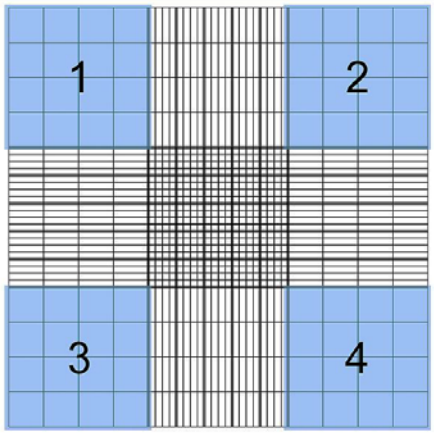

Figure 10: Grid layout, modified from Microbehunter - Microscopy Magazine, June 27th 2010

To determine cell numbers a Neubauer-improved-hemocytometer was used. 10µl of the cell suspension was pipetted under the glass plate and cells from all four 4x4 squares were counted under a light microscope using a 40x objective. The concentration (cells/ml) was calculated with the following formula:

$$\boldsymbol{Concentration} = \frac{\boldsymbol{Number\ of\ cells\ x\ 10.000}}{\boldsymbol{4}}$$

2.1.4 Freezing cells

Semi-confluent cells were trypsinized as stated before. The cell suspension was collected in a 15ml falcon tube. Cells were pelleted by centrifugation at 300g for 6 minutes and resuspended in medium supplemented with 10% DMSO. The volume was chosen to obtain approximately $1x10^6$ cells/ml. 1ml was transferred into a cryotube and frozen slowly at -80°C in a box containing isopropanol. For long-time storage cells were placed into a liquid nitrogen tank the following day.

2.1.5 Thawing cells

Cryotubes were taken out of the liquid nitrogen tank and thawed at 37°C. The suspension was taken up into 3ml appropriate medium and transferred into a 15ml Falcon tube. The cells were pelleted by centrifugation at 300g for 6 minutes, were washed once with 4ml 1xPBS/EDTA to remove traces of remaining DMSO and centrifuged again. After the

removal of PBS/EDTA the pellet was resuspended in a final volume of complete medium and plated onto a cell culture dish.

2.1.6 Transient transfection

Cells were seeded in 60mm plates and let adhere overnight. When cells reached 50 to 80% density, transfection was performed using CalPhos™ Mammalian Transfection Kit (Clonetech, #631312). 5µg of DNA was brought to a volume of 438µl with sterile water. 62µl 2M calcium chloride was added dropwise and the solutions were mixed by inverting several times. 500µl 2xHBS (HEPES plus additives) solution was added dropwise and incubated for 15 minutes at room temperature. The total volume of 1ml was then added dropwise to the plate containing 3ml medium and mixed by gentle moving up and down. Medium was changed 16 hours later after checking for precipitate formation and expression was analyzed 48 hours post transfection.

2.1.7 Stable transfection

Cells were seeded as described above. Before transfection, medium was exchanged with 3mL fresh medium. 6µl of Fugene6 Reagent (Promega, E2691) was added to 94µl of serum-free medium. 2µg of the plasmid-DNA was added and mixed by tapping. The solution was incubated at room temperature for 40 minutes and then added dropwise to the plate. 72 hours post transfection selection for stable clones was started with 600µg/ml of G418 for several weeks.

2.1.8 Lentiviral transduction

RNA interference mediated downregulation of TUSC3 was performed by lentiviral delivery using TRC Lentiviral Human TUSC3 shRNA (Open Biosystems, Thermo Fisher Scientific, TRCN0000038064) and HEK293 cells as packaging cell line. In a first step HEK293 cells were transiently transfected as reported above with 5µg of each lentiviral particle (VSV-G, RGR and RSV) plus the shRNA-construct. After incubation overnight, medium was exchanged by 2ml of fresh DMEM. 48 hours post transfection medium was collected with a syringe and filtered through a 0.45µm filter. Fresh medium of the same volume as collected was added, as well as polyprene to a final concentration of 8µg/ml. The cocktail,

containing viral particles, was applied to prostate target cells to be stably transduced for at least 8 hours in two rounds with changing to normal growth medium in-between for at least 18 hours to let the cells recover. Selection for positive transfectants was initiated 48 hours after infection using 3µg/ml puromycin for several weeks.

2.1.9 Cell viability assay

Cells were plated in triplicates at a density of 5×103 cells in 100µl of culture medium to a 96-well plate and were left overnight to adhere. On the next day medium was aspirated, cells were washed once with 200µl 1xPBS/EDTA and an appropriate amount of medium with additives was added again. Cells were then incubated for 24 to 72 hours. For measuring cell viability 20µl of Cell Titer Blue Viability reagent (Promega, G8081) were added to each well and incubated for 3 to 4 hours at 37°C in a humidified incubator which leads to a color change of the medium depending on the number of metabolic active (viable) cells. Fluorescence was measured at two wavelengths (560 and 590nm) on a multimode microplate reader (Berthold Technologies, Tristar LB-941).

2.1.10 Cell invasion assay

5×10^4 cells were seeded in serum-free medium onto a 24-well plate with modified Boyden chambers (BD Biosciences, BD BioCoat™ BD Matrigel™ Invasion Chamber). The lower chamber contained culture medium supplemented with 20% FBS as a chemoattractant. Cells were incubated for 18 hours at 37°C in a humidified incubator. Afterwards, cells that have been stuck in the 8µm pores of the modified Boyden chambers were stained with 0.05% crystal violet and counted under a light microscope (Zeiss, Axiovert 40CFL).

2.1.11 Luciferase assay

Luciferase Assay Systems (Promega, E1531) was performed according to manufacturer's protocol. Stably transfected cells were seeded at a density of $5x10^3$ cells/well to a 96-well plate and let adhere overnight. The next day, growth medium was removed and cells were washed once with 1xPBS. Cells were lysed by the addition of 20µl 1xLysis Reagent (Promega, CCLR). A multimode microplate reader (Berthold Technologies, Tristar LB-

941) dispensed automatically 100µl of Luciferase Assay Reagent and measured the intensity of light produced.

2.1.12 Scratch assay

$6x10^4$ cells were seeded to each well of a 96-well plate to reach a monolayer the next day. Scratches were produced by using a 96-well Wound Maker (Essen Bioscience) followed by two washing steps with 1xPBS/EDTA. Medium containing 5ng/ml mitomycin c to inhibit proliferation was added and incubation was continued at 37°C in a humidified atmosphere with 5% CO_2. Wound closure was followed and analyzed by use of the IncuCyte ZOOM system (Essen Bioscience).

2.2 Immunoblot

2.2.1 Antibodies and lectins

Table 1: HRP-conjugated primary antibodies (* same manufacturer)

Name	Company	Type	Host	Size	Dilution
CD44	abcam, 51037	Monoclonal	rabbit	82kDa	1:1000
CHOP	Thermo Scientific, 9C8	Monoclonal	mouse	31kDa	1:500
E-Cadherin	BD Bioscience, 610181	Monoclonal	mouse	120kDa	1:1000
EGFR	Santa Cruz Laboratories, sc-03	Polyclonal	rabbit	175kDa	1:300
IGF-Iβ	Cell Signaling, #9750	Monoclonal	rabbit	95kDa	1:1000
Integrin-β_1	R&D Systems, AF1778	Polyclonal	goat	135kDa	1:1000
Luciferase	Millipore, AB3256	Polyclonal	goat	63kDa	1:10,000
Phospho-Akt	Cell Signaling, #4060	Monoclonal	rabbit	60kDa	1:1000
STT3A	Novus Biologicals, H00003703-A01	Polyclonal	mouse	81kDa	1:500
STT3B	Proteintech, 15323-1-AP	Polyclonal	rabbit	94kDa	1:1000
Total-Akt	Cell Signaling, #9272	Polyclonal	rabbit	60kDa	1:1000
TUSC3	Novus Biologicals, NBP1-55630	Polyclonal	rabbit	39kDa	1:500
TUSC3	Santa Cruz, sc-98192	Polyclonal	goat	43kDa	1:200
TUSC3*	abcam, 65213	Polyclonal	rabbit	40kDa	1:500

TUSC3*	Sigma-Aldrich, SAB4503183	Polyclonal	rabbit	40kDa	1:500
β-Tubulin	Sigma-Aldrich, T4026	Monoclonal	mouse	55kDa	1:1000
β-Actin (I-19)	Santa Cruz, sc-1616	Polyclonal	goat	42kDa	1:1000

Table 2: HRP-conjugated secondary antibodies and unconjugated isotype control

Name	Company	IgG	Host	Dilution
donkey anti-goat	Santa Cruz Laboratories, sc-2020	goat	donkey	1:5000
goat anti-mouse	Santa Cruz Laboratories, sc-2005	mouse	goat	1:5000
goat anti-rabbit	Santa Cruz Laboratories, sc-2004	rabbit	goat	1:5000
normal rabbit-IgG	Santa Cruz Laboratories, sc-2027	rabbit	rabbit	/

Table 3: HRP-conjugated lectins

Name	Company	Origin	Recognizes
Canavalia ensiformis Concanavalin A	USBiological, C1045-20	Jackbean	galactose, mannose or glucose
Phaseolus vulgaris L PHA-L	USBiological, P3370-55	Red Kidney Bean	galactose, N-acetylglucosamine, and mannose

2.2.2 Buffers and reagents

10xRunning Buffer (25mM Tris, 192mM Glycin, 0.1%SDS); 30% Acrylamid/bis-Acrylamid solution (Sigma-Aldrich, A3574); Ammonium persulfate (Sigma-Aldrich, A3678); Anode Buffer I (0.3M Tris, 10% Methanol); Anode Buffer II (25mM Tris, 10% Methanol); Bovine Serum Albumin (Sigma, A9418); Cathode Buffer (25mM Tris, 40mM Glycin, 10% Methanol); cOmplete ULTRA Tablets (Roche, 05892791001); Laemmli Loading Buffer (300mM Tris-HCl (pH=6.8), 50% Glycerol, 10% SDS, 0.05% Bromphenolblue, 0,1M DTT); Methanol (Merck, MCK1060091000); Non-fat dry milk powder (AppliChem, A0830); NP-40 Alternative (Calbiochem, 492016); nProtein A Sepharose 4 Fast Flow (GE Healthcare, 17-5280-01); PhosSTOP Phosphatase Inhibitor Cocktail Tablets (Roche, 04906837001); Pierce ECL Western Blotting Substrate (Thermo Scientific, 32106); RIPA lysis buffer (50mM Tris-HCl pH=7.4, 150mM NaCl, 50mM NaF, 1mM EDTA, 1% NP-40).

2.2.3 Protein isolation and measurement

Cells from a semi-confluent 6-well plate were washed once with ice-cold 1xPBS to remove remaining medium. 200µl RIPA lysis buffer, with freshly added protease (stock solution: 50x) and phosphatase (stock solution: 10x) inhibitors, was added to each well and left on ice for 5 minutes. The cells were scratched off the plate with a plastic cell scraper and collected in a pre-cooled 1.5ml tube. The tube was incubated on ice for another 10 minutes and centrifuged with 18,000g for 15 minutes at 4°C. The supernatant (protein fraction) was collected for protein concentration measurement using Bradford Reagent Assay (Thermo Scientific). 795µl of the reagent were put into a plastic cuvette and 5µl of each protein sample was added. Upon careful mixing, the absorbance at 595nm was measured after 5 minutes on a spectrometer (Hitachi, U-2900). Simultaneously, a standard curve was produced with BSA samples in a dilution range from 0 to 2µg/ml to calculate protein concentrations by using the resulting trendline.

2.2.4 Sodium dodecyl sulfate polyacrylamide gel electrophoresis (SDS-PAGE)

Table 4: Recipes for preparing one polyacrylamidgel for Tris-glycine SDS-PAGE

Resolving Gel	8%	10%	12%
H2O	2.3mL	1.9mL	1.6mL
30% Acrylamide/ bis-Acrylamide	1.3mL	1.7mL	2.0mL
1,5 M Tris-HCl (pH 8.8)	1.3mL	1.3mL	1.3mL
10% SDS	50µL	50µL	50µL
10% Ammonium persulfate	50µL	50µL	50µL
TEMED	3µL	2µL	2µL

Stacking Gel	5%
H2O	1.4 mL
30% Acrylamide/ bis-Acrylamide	330µL
1M Tris-HCl (pH 6.8)	250µL
10% SDS	20µL
10% Ammonium persulfate	20µL
TEMED	2µL

Loading Buffer modified from Laemmli (Laemmli, 1970) was added to 15µg-30µg protein and the sample was heated for 5 minutes at 95°C. The same amount of protein from each sample was loaded into one well and the run was started with 100V until the color-dye

front passed the stacking gel. Afterwards the run was accelerated with 150V and stopped before the loading dye ran out of the gel.

2.2.5 Western Blotting

The gel was equilibrated in Anode Buffer I with one filter paper. Two other filter papers were soaked into Anode Buffer II and three others were placed in Cathode Buffer. PVDF membrane was activated in pure methanol for one minute. A sandwich was built in the following order: 2x filterpapers (Anode Buffer II), 1x filterpaper (Anode Buffer I), membrane, gel, 3x filterpapers (Cathode Buffer). Blotting was performed for 45 minutes at 17V on a semi-dry blotting sytems (Bio-Rad, Transfer-Blot SD Semi-Dry Transfer Cell). After blotting, the gel was washed in 1xPBS/Tween-20 (0.1%) and blocked in 5% non-fat dry milk or 5% BSA/PBS-0.1%Tween-20 (for phosphoproteins) at room temperature (RT) for 60 minutes under gentle shaking. Incubation with primary antibody was performed overnight at 4°C under gentle shaking. After incubation, the membrane was washed 3 times for 5 minutes with 1xPBS/Tween-20 (0.1%) and incubated with secondary antibody (diluted in 1% non-fat dry milk) for 90 minutes at RT under gentle shaking. Finally, the gel was washed 5 times for 10 minutes with 1xPBS/Tween-20 (0.1%) under gentle shaking. ECL detection reagent was mixed 1:1 and a sufficient amount was placed on the membrane and kept on it for one minute. The solution was poured off the membrane; the membrane was wrapped into a plastic sheet, and developed digitally using BIORAD ChemiDoc^{TM} XRS+.

2.2.6 Eastern Blotting

After polyacrylamide gel electrophoresis and conventional western blotting, the PVDF-membrane was blocked either in 1xPBS/Tween-20 (0.5%) or 1%BSA/PBS-0.1%Tween-20 for 1 hour under gentle agitation. Incubation with the HRP-conjugated lectin was performed in blocking solution for at least 2 hours. The membrane was washed for 60 minutes with 6 changes in blocking solution and developed by chemiluminescence as stated before.

2.2.7 Co-Immunoprecipitation

Cells were lysed in a gentle lysis buffer (1xPBS/0.75% NP-40 plus 1xprotease and 1xphosphatase inhibitors) and 500µg of protein were brought to a volume of 400µl with lysis buffer. A pre-clearing step was performed by the addition of 20µl nProtein A Sepharose 4 Fast Flow beads and incubation for 1 hour at 4°C under gentle rotation. The beads were pelleted by short centrifugation and the supernatant was incubated over night at 4°C with 2µg of the primary antibody or normal rabbit IgG. After the addition of 40µl nProtein A Sepharose 4 Fast Flow beads, the incubation time was continued for 150 minutes at 4°C under gentle rotation. Beads were collected by centrifugation at 6,000g for 2 minutes. The supernatant was removed carefully, followed by three washing steps with cooled Washing-Buffer (1xPBS, 0.5% NP-40) for 5 minutes each on a rotator. The beads were resuspended in 25µl of 2xLoading Buffer and heated for 10 minutes at 95°C. The sample was centrifuged for 2 minutes with 6,000g and 20µl of the supernatant was used for Western Blot analysis.

2.3 Cloning

2.3.1 Plasmids & reagents

50xTAE Buffer (2M Tris, 1M acetic acid, 50mM EDTA); Ampicillin sodium salt (Sigma Aldrich, A0166); competent DH5α™ cells (Invitrogen, 18258-012); dNTP Mix (Invitrogen, 46-0344); EcoRI (New England Biolabs (NEB, R0101S); GelRed™ (Biotium, 10,000x in H_2O); HindIII (NEB, R0104S); Kanamycin disulfate salt from Streptomyces kanamyceticus (Sigma Aldrich, K1876); LB Agar (Sigma Aldrich, L2897); LE Agarose (Biozym, 840004); Lennox L Broth Base (Invitrogen, 12780-052); NEBuffer 2 (NEB, B7002S); pcDNA3.1+ (Invitrogen, V790-20); pDsRed-ER, a kind gift from Karin Nowikovsky (Medical University of Vienna, Austria); pEGFP (Clontech, #6084-1); QIAGEN Plasmid Maxi Kit (Qiagen, 12163); Quick Ligation™ Kit (New England BioLabs, M2200S); SOC-Medium (Sigma, S1797); TUSC3image_pcDNA3.1(+), generated during previous studies; Wizard®Plus SV Minipreps DNA Purification System (Promega, A1460).

2.3.2 Restriction Digest

Table 5: Restriction Master Mix

	1x
DNA	500ng
10x NEB Buffer 2	2µL
HindIII	0.5µL
EcoRI	0.5µL
BSA	0.2µL
H_2O	16.8µL
Total	20µL

A fragment containing the TUSC3 cDNA was cut out of a previously generated expression vector with the two endonucleases HindIII and EcoRI. The target vector pEGFP-C1 was digested with the same enzymes. Restriction digest was performed for 90 minutes at 37°C according to the manufacture's recommendation. 5µl were loaded on a 1% agarose gel to confirm successful restriction. 0.4g agarose was dissolved in 40ml 1xTAE Buffer by briefly cooking in a microwave. To visualize nucleic acids under UV light, 1.5µl of GelRed™ was added to the hand-warm gel, which was casted into a 7x10cm gel tray with a 8-well comb inside. Electrophoresis was performed for 60minutes with 80V in a BIORAD Mini-Sub Cell GT System. For ligation 10µl without loading dye were separated by electrophoresis and the desired band was cut out of the gel under UV-light using BIORAD ChemiDoc™ XRS+.

2.3.3 Gel purification

Gel purification was performed using Illustra's GFX PCR DNA and Gel Band Purification Kit. The band of interest was excised under UV-light and placed into a microcentrifuge tube. 500µl Capture buffer type 3 was added and heated at 60°C, until agarose was completely dissolved. The sample-mix was transferred into MicroSpinTM column placed into a collection tube. After waiting for 60 seconds the tube was centrifuged for 30 seconds with 16,000g. The flow-through was discarded and the column was placed back into the collection tube. The column was washed once with 500µl Washing buffer type 1 and centrifuged again with 16,000g for 30 seconds. The collection tube was discarded and the column was placed into a new microcentrifuge tube. The DNA was eluted by the addition of 25µl Elution buffer type 4 and after incubation for 60 seconds by centrifugation with 16,000g for 2 minutes.

2.3.4 Ligation

50ng of the purified vector was combined with 3-fold molar excess of purified insert. The volume was adjusted to 10µl with dH20 and mixed with 10µl of 2x Quick Ligation Buffer. After the addition of 1µl Quick T4 DNA Ligase, the sample was mixed thoroughly and centrifuged briefly. The mixture was incubated for 5 minutes at 25°C on an Eppendorf Thermocycler, and chilled on ice afterwards.

2.3.5 Transformation

50µl of competent DH5α™ cells were mixed with 15µl of the ligation product in a 1.5ml tube. The mixture was stored 20 minutes on ice and afterwards heat-activated for 45 seconds at 42°C and placed immediately back on ice for another 2 minutes. 500µl of SOC-Medium was added to the tube and the bacteria were incubated for 1 hour at 37°C under rocking with 1,000rpm. The cells were pelleted by centrifugation at 5,000g for 5 minutes. The pellet was resuspended in 100µl of supernatant and put onto a LB-Agar plate containing antibiotics (100µg/ml Ampicillin or 50µg/ml Kanamycin). The plate was incubated bottom-up at 37°C overnight.

2.3.6 Plasmid preparation

A single colony was picked from the plate to inoculate a starter culture of 3 ml LB media (20g/l of Lennox L Broth Base) containing respective antibiotics in the same concentration as on plate. The culture was incubated for approximately 8 hours at 37°C with vigorous shaking and later 200µl of the suspension was used to inoculate a volume of 200ml and continuing incubating overnight. The next day, bacteria were harvested by centrifugation at 6,000g for 15 min at 4°C. For the plasmid preparation, the QIAGEN Plasmid Maxi Kit was used. The bacterial pellet was resuspended thoroughly in 10ml of buffer P1, followed by the addition of 10ml buffer P2. The suspension was mixed by inverting several times and incubated for 5 minutes at RT. After the addition of 10ml chilled buffer P3 incubation was continued for 20 minutes on ice. The lysate was cleared by two centrifugation steps a 20,000g at 4°C, the first time for 30 minutes, the second time for 15 minutes. In the meantime, a column was equilibrated by applying 10ml of buffer QBT and afterwards the

cleared supernatant was applied to it. The column was washed two times with 30ml of buffer QC and finally the DNA was eluted with 15ml buffer QF. DNA was precipitated by the addition of 10.5ml isopropanol and pelleted by centrifugation immediately at 15,000g for 30 minutes at 4°C. The DNA pellet was washed once with 5ml 70% ethanol and centrifuged again at 15,000g for 10 minutes at 4°C. After air-drying the pellet for at least 10 minutes, DNA was resuspended in 250µl ribonuclease-free water. DNA concentration was measured on a Nanodrop 8000 (Thermo Scientific).

2.4 Polymerase Chain Reaction

2.4.1 Primer probes

Table 6: Primers used for semi-quantitative PCR and qRT-PCR

Name	Source	Additional Information
XBP-1_for	(Samali et al., 2010)	TTA CGA GAG AAA ACT CAT GGC C
XBP-1_rev	(Samali et al., 2010)	GGG TCC AAG TTG TCC AGA ATG C
TUSC3	Applied Biosystems, Life Technologies	Hs00185147_m1
MagT1	Applied Biosystems, Life Technologies	Hs00259564_m1
EGFR	Applied Biosystems, Life Technologies	Hs00193306_m1
HPRT1	Applied Biosystems, Life Technologies	Hs99999909_m1

2.4.2 Reagents

6x DNA Loading Dye (0.25% bromophenol blue, 0.25% xylene cyanol FF, 30% glycerol in water); Chloroform (Applied Biosystems, 400459); Isopropanol (Merck, K40027034); RNAzol® RT (Molecular Research Center, Inc.); Taq DNA polymerase (NEB, M0267L); TaqMan® Universal PCR Master Mix (Applied Biosystems, Life Technologies, 4324018); ThermoPol® Reaction Buffer (NEB, B9004S).

2.4.3 RNA isolation

Total RNA was isolated from a semi-confluent 6-well plate by adding 500µl of RNAzol® RT, followed by 5 minutes incubation at room temperature. The homogenate was transferred to a pre-cooled 1.5ml tube and 100µl chloroform was added. After vigorously mixing, the sample was placed on ice for 15 minutes. Then, the sample was centrifuged for 15 minutes at 12,000g at 4°C. Afterwards the aqueous phase was transferred to a new clean tube and RNA was precipitated by adding 300µl isopropanol. The solution was mixed and placed on ice for another 15 minutes. RNA was pelleted by centrifugation with 12,000g for 8 minutes at 4°C. The pellet was washed once with 75% ethanol and centrifuged again at 7,500g for 5 minutes at 4°C. The pellet was air-dried for 10 minutes and resuspended in RNase-free water at 60°C. RNA concentration was measured on a Nanodrop 8000 UV-Vis Spectrophotometer (Thermo Scientific) by using 1.5µl of each sample.

2.4.4 cDNA synthesis

cDNA was synthesized from 5µg of total RNA in a volume of 20µl using the SuperScript® First-Strand Synthesis System for RT-PCR (Invitrogen). First the volume of the RNA was filled to 10µl with RNAse-free water and 1µl Oligod(T) primers and 1µl dNTP mix were added to a PCR-tube. The mixture was heated to 65°C on a thermocycler and quickly chilled on ice. The content was collected by brief centrifugation and 4µl 5xFirst-Strand Buffer and 2µl 0.1M DTT were added. The mixture was incubated for 2 minutes at 42°C. In the last step 1µl of SuperScript™ II RT was added and incubation was continued for 50min at 42°C. The reaction was inactivated by heating up to 70°C for 15 minutes. The volume was filled up to 100µl by the addition of 79µl ddH2O and the sample was stored at -20°C.

2.4.5 Semi-quantitative Polymerase Chain Reaction

Table 7: The following PCR master mix was prepared with reagents from NEB

	1x
cDNA Template	5µl
10x Standard Taq Buffer	2,5µl
25mM MgCl2	2µl
2.5mM dNTPs	2µl
20µM Forward Primer	1µl
20µM Reverse Primer	1µl
Taq DNA Polymerase	0.2µl
ddH_2O	11.3µl
Total	25µl

Table 8: The following cycling program has been used for all PCR reactions

Step	Temperature	Duration
1	94°	5min
2	94°	30sec
3	58°	30sec
4	68°	30sec
5	68°	10min
6	4°	∞

Reaction was stopped after 32 cycles, and 4µl of 6xDNA Loading Dye was added to each sample. To confirm PCR products, 12µl were loaded to a 1.5% agarose gel. Gel electrophoresis was performed as stated elsewhere (2.3.2).

2.4.6 Quantitative realtime Polymerase Chain Reaction (qRT-PCR)

qRT-PCR was performed using TaqMan® Gene Expression Assay with FAM-conjugated Assay-on-Demand™ probes (Applied Biosystems, Life Technologies). All PCR reactions were performed in triplicates with negative controls included. The reaction mixture was comprised of 10µl TaqMan® Universal PCR Master Mix, 2µl of the cDNA obtained, 1µl of the respective TaqMan Assay Probe and 7µl of ddH_2O to give a total volume of 20µl. The reaction was performed on a StepOne™ Plus Real-Time PCR System (Applied Biosystems, Life Technologies) with default settings. Relative expression values were determined using the ΔΔCT method, obtained by the StepOne™ Software v2.1 (Applied Biosystems, Life Technologies).

2.5 Cell imaging techniques

2.5.1 Buffers and reagents

10% Formalin, neutral buffered (10% formaldehyde, 46mM NaH_2PO_4 (anhydrous), 29mM NaH_2PO_4); 4',6-Diamidino-2-Phenylindole (DAPI) (Invitrogen, D1306), was a kind gift from Karin Nowikovsky (Medical University of Vienna, Austria); Eukitt® quick-hardening mounting medium (Sigma-Aldrich, 03989); Fluorescence Mounting Solution (Dako, S3023); Formaldehyde solution (Sigma-Aldrich, F-8775); Liquid DAB+ Substrate Chromogen System (Dako, K3468); Triton-X (Sigma-Aldrich, T8787).

2.5.2 Fluorescence microscopy

$5x10^4$ cells were seeded onto cover slips in a 24-well plate. After cell attachment, they were transfected with plasmids carrying proteins with fluorescent tags using the FuGene 6 reagent as described earlier (see 2.1.8). After 72 hours cells were fixed with 4% paraformaldehyde for 10 minutes at room temperature and washed twice with 1xPBS for 5 minutes. Cells were permeabilized with 0.25% Triton-X/PBS for 10 minutes at RT and washed three times with 1xPBS for 5 minutes, followed by the incubation with DAPI (1µg/ml) for 2 minutes in dark. Solution was soaked off and cover slips were mounted on a glass slide. Mounting solution was dried over-night at room temperature in dark and cells were visualized using laser scanning microscopy (Zeiss LSM700).

2.5.3 Lectin-based cytochemistry

$5x10^3$ cells were seeded into an 8-well chamber slide (Nunc® Lab-Tek® Chamber Slide™ system, Sigma-Aldrich) and cells were grown to reach 70% to 80% confluency. Medium was soaked off, cells were washed once with 1xPBS and fixed by the addition of 10% formalin for 10 minutes at room temperature. Formalin was removed by two additional washing steps with 1xPBS for 5 minutes and cells were permeabilized with 0.1% Triton-X/PBS for 10 minutes at room temperature and washed again extensively three times with 1xPBS for 5 minutes each. Cells were blocked in 5% BSA/PBS for 30 minutes and incubated with Concanavalin A (ConA-HRP) (dilution 1:40) for 2 hours at 4°C. Unbound

lectins were removed by six washing steps with 1xPBS/Tween-20 (0.1%) for 5 minutes each. Lectin staining was visualized by incubation with 3,3-diaminobenzidine-(DAB) hydrogen peroxide for 30 seconds at room temperature. Thereafter, the slide was rinsed for 5 minutes in distilled water, counterstained with haematoxylin for 1 minute, rinsed again in water for 5 minutes and dehydrated in a graded alcohol series (70%, 85% and 100%, 1 minute each). The slide was mounted with Eukitt solution, covered with a cover slip and analyzed under a light microscope (AxioImager, Zeiss).

2.6 Mouse experiments

2.6.1 Xenografts

$1x10^7$ cells of control or shRNA TUSC3 DU145 and $5x10^6$ cells of PC3 were subcutaneously injected either into the right or the left dorsal flank of five 8-week old male, athymic Foxn1nu/nu mice. PC3 cells were mixed with Matrigel (BD Biosciences) in a 1:1 volume ratio for proper engraftment. Tumor size was measured three times a week in two perpendicular axes by using a caliper and tumor volume was calculated with the formula:

$$\boldsymbol{volume} = \frac{\boldsymbol{length\ x\ width^2}}{\mathbf{2}}$$

Animal experiments were done according to protocols approved by the Austrian Federal Ministry for Science and Research and mice were maintained under specific pathogen-free conditions.

2.6.2 RNA isolation from tumors

Half of the isolated tumors were homogenized in 1mL RNAzol RT at 4°C, using a Potter-Elvehjem homogenizer (Kimble Chase) with several strokes at 15,000 rpm until no clumps were visible. RNA isolation protocol was followed as stated elsewhere (2.4.2).

3 Results

3.1 Carcinogenesis

3.1.1 Silencing TUSC3 in prostate cancer cell lines

To mimic tumor suppressive conditions, TUSC3 was knocked down in two well established androgen resistant prostate cancer cell lines, DU145 and PC3. To achieve stable silencing of TUSC3, we used lentiviral mediated transduction with a specific shRNA construct targeting TUSC3 (shTUSC3). Non-targeting shRNA, sh-scrambled (shscr), was used as control. The silencing efficiency was confirmed on the mRNA expression level by qRT-PCR and on protein level by Western Blot analysis (Figure 11). TUSC3 expression was reduced to approx. 20% in DU145 and to approx. 5% in PC3 when comparing shTUSC3 knockdown to shscr control cells. Interestingly, protein analysis revealed a less effective knockdown. As for the mRNA expression, the effect is more pronounced for DU145 cells than for PC3 cells at the protein level (see also Suppl. Data, Table 9). In general, TUSC3 immunoblotting turned out to be challenging and hardly reproducible. None of the four tested antibodies from different companies were giving a clear result and none of them has been referenced in any publications yet.

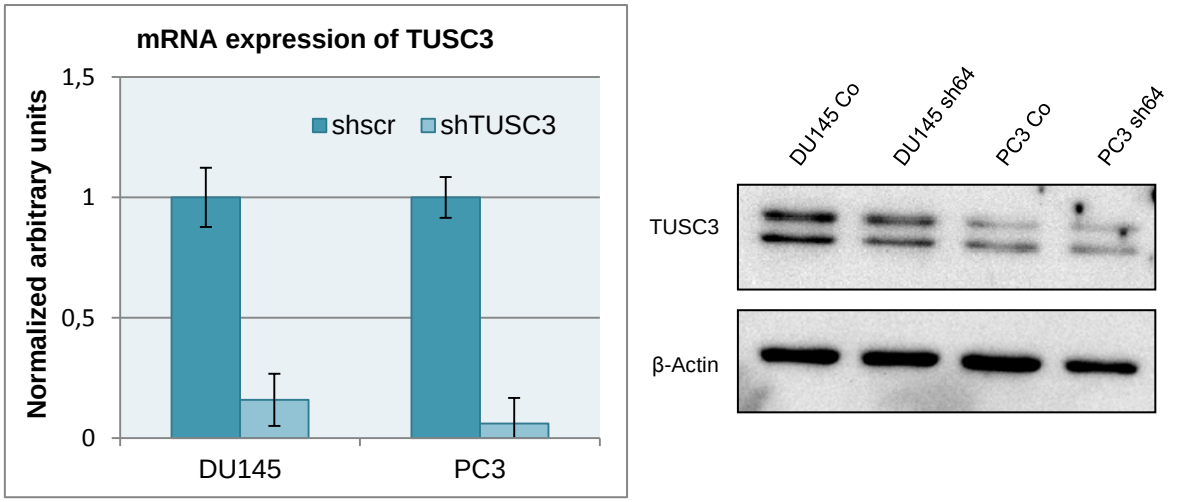

Figure 11: TUSC3 knockdown on the mRNA (left) and protein (right) level in DU145 and PC3 cells. TUSC3 mRNA expression was measured by qRT-PCR. Data was normalized to hypoxanthin-guanin-phosphoribosyltransferase 1 (HPRT1) expression as housekeeping gene while TUSC3 expression in shscr cells was set as one. Error bars represent the standard deviation of the mean (n=3). A representative Immunoblot is shown by using TUSC3-Antibody from Sigma-Aldrich (SAB4503183, dilution 1:500) and Anti-Actin from Santa-Cruz (sc-1616, 1:1000) as loading control. The quantitation of protein levels are given in the Supplemental Data (Table 9).

Nevertheless, we obtained the best result using the TUSC3 antibody from Sigma-Aldrich, though we detected a double-band at the estimated height of 40kDa (Figure 11). We hypothesized that the antibody also recognizes MagT1, a close TUSC3 paralogue in human which differs in size by 1 kDa. Quantitative determination of MagT1 mRNA by qRT-PCR revealed unchanged levels of MagT1 (Suppl. Figure 1). With the intention to correlate one of the bands with TUSC3, we transiently transfected HEK293 cells with a plasmid containing the TUSC3 cDNA. Similarly, we could demonstrate an enormous TUSC3 overexpression on the mRNA level, but not on the protein level (Figure 12). Both bands were affected by TUSC3 overexpression, for which reason it is not possible to exclude one of them. Indeed, TUSC3 exists in two isoforms, but they just differ by one amino acid in length which alone cannot explain the second band on the blot. Protein modifications affecting protein stability and mobility could serve as another explanation for the second detected band. According to PhosphoSitePlus® (Hornbeck et al., 2012) TUSC3 contains six possible phosphorylation sites and three N-glycosylation sites (Zhang et al., 2006). Nevertheless, an effective use of these sites is still unclear, because many of them are located at transmembrane regions.

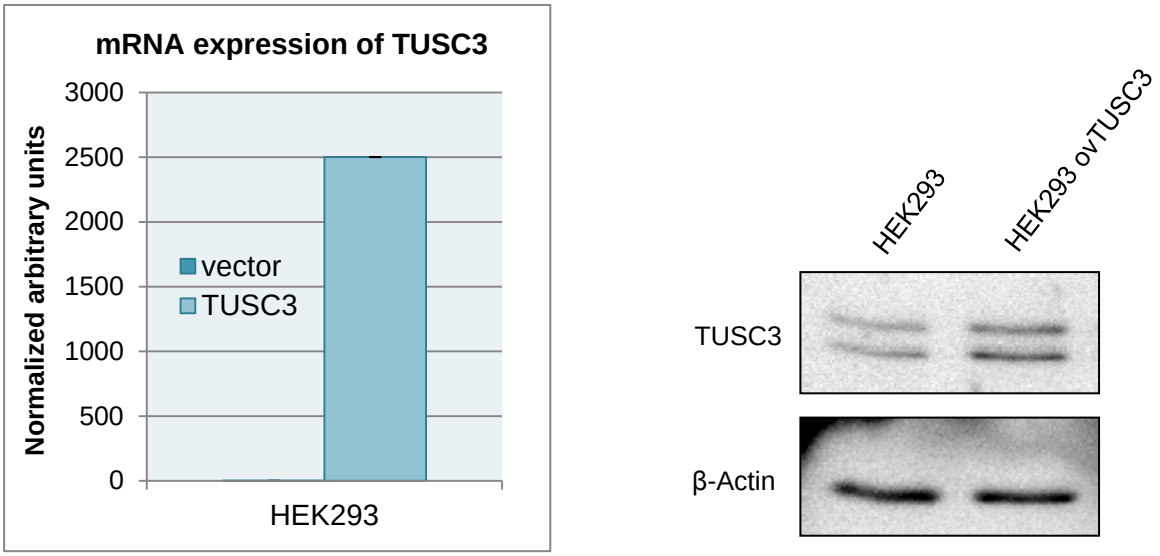

Figure 12: Overexpression of TUSC3 in HEK293 cells. HEK293 cells were transiently transfected with a plasmid containing the TUSC3 cDNA by using the calcium phosphate method. Left panel: TUSC3 mRNA expression was measured by qRT-PCR and normalized to the expression of HRPT1. Expression of TUSC3 in HEK293 cells, transfected with the empty plasmid, was set as one (not visible in the graph). Error bars represent the standard deviation of the mean (n=3). TUSC3 expression was 2500 fold higher in TUSC3 overexpressing cells. Right panel: The protein expression level obtained by immunoblotting with anti-TUSC3 antibody (Sigma Aldrich, 1:500) does not correspond to this value. The quantitation of protein levels are given in the Supplemental Data (Table 9).

3.1.2 Effects of TUSC3 knockdown on viability of prostate cancer cell lines

First we addressed the question, whether reduced expression of TUSC3 has an effect on the viability of prostate cancer cells. Therefore, we performed a viability assay based on the measurement of the metabolic capacity of cells to reduce resazurin to resorufin. Only resorufin is highly fluorescent, thus enabling to determine the number of living cells by the fluorescent signal generated after a given time frame. Indeed, we observed an increase in fluorescence, ergo viability, of TUSC3 silenced PC3 cells after 72 hours compared to control cells (Figure 13D) and a retained growth advantage of these cells even under serum deprivation (Figure 13C). However, DU145 cell viability was not affected by TUSC3 (Figure 13A+B), indicating a TUSC3 specific function in the heterogeneity of prostate cancer. Alterations in cell viability can be either explained by an increase of cell proliferation or a decrease of cell death. Both mechanisms are hallmarks of cancer cells and an influence of TUSC3 on either of these processes needs to be further studied.

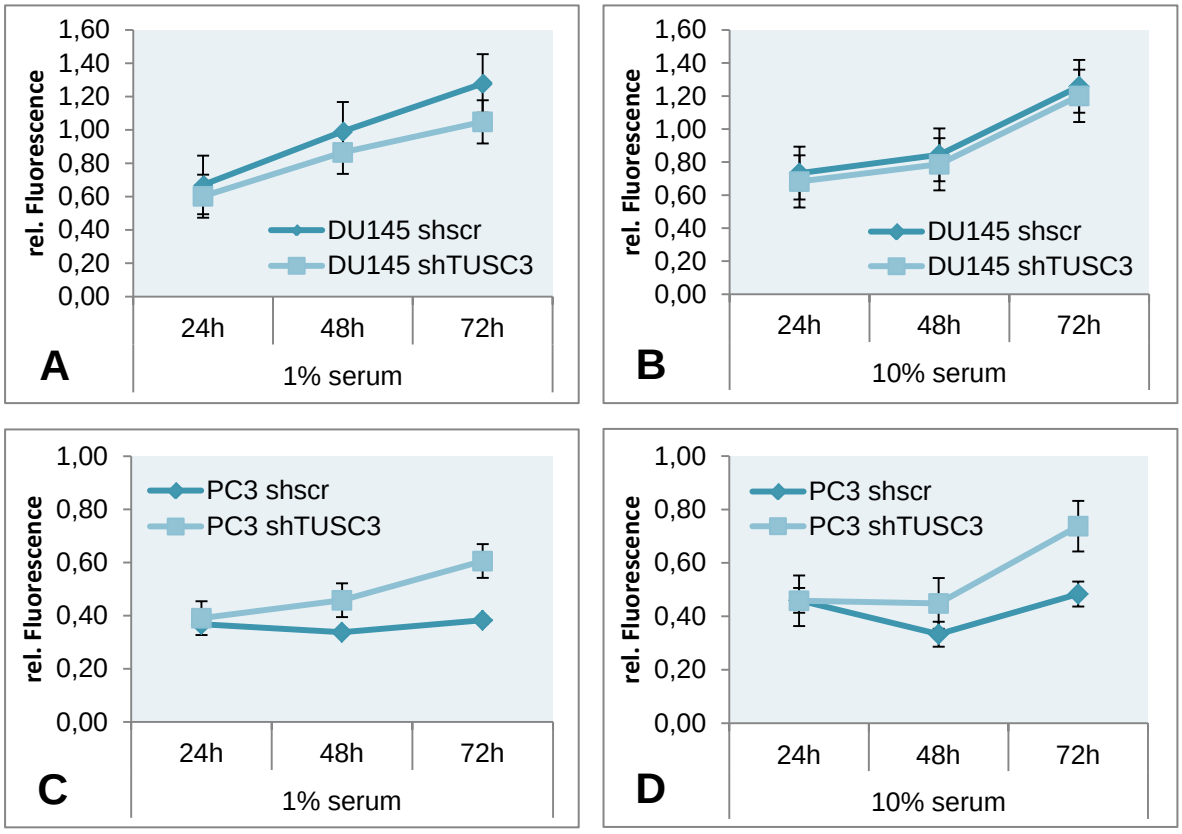

Figure 13: Cell viability of prostate cancer cell lines in the presence of serum and under serum starvation. Cells were plated in triplicates at a density of 5000 cells per well on a 96-well plate. The next day, medium was exchanged and the amount of cells in each well was detected by measuring fluorescence at 560 and 590nm after the addition of Cell Titer Blue Reagent (Promega) and an incubation time of 4 hours. These values were used to standardize the values measured after 24, 48 and 72 hours from separate plates. Error bars represent the standard deviation of the mean (n=3).

3.1.3 Tumor growth in nude mice

We injected the two prostate cancer cell lines into male nude athymic (Foxn1nu/nu) mice. Tumors from DU145 cells showed no difference in tumor size or growth rate dependent on TUSC3. However, xenografts derived from PC3 shTUSC3 developed a growth advantage compared to their control counterparts after 6 to 7 weeks (Figure 14, Figure 15 bottom left and middle panel). We isolated RNA from xenograft tumors and could demonstrate that shTUSC3 cells injected into the right flank showed reduced TUSC3 expression compared to shscr cells injected into the left flank (Figure 15, right panel). Furthermore, immunohistochemical staining confirmed that protein expression of TUSC3 was lower in shTUSC3 tumors (Figure 15, upper left panel). Animal experiments were carried out by the professional technical support of Martin Holcmann and Martina Hammer (Institute of Cancer Research, Vienna, Austria), Dr. Roberto Plasenzotti and Ing. Astrid Fabry (Institute of Biomedical Research, Medical University of Vienna (MUW), Austria), and Dr. Peter Horak (Clinic for Internal Medicine I, MUW, Austria). Immunohistochemical staining was done with the help of Prof. Reinhard Horvat (Clinical Department of Pathology, MUW, Austria) and Dr. Mariam Anees (Clinic for Internal Medicine I, MUW, Austria).

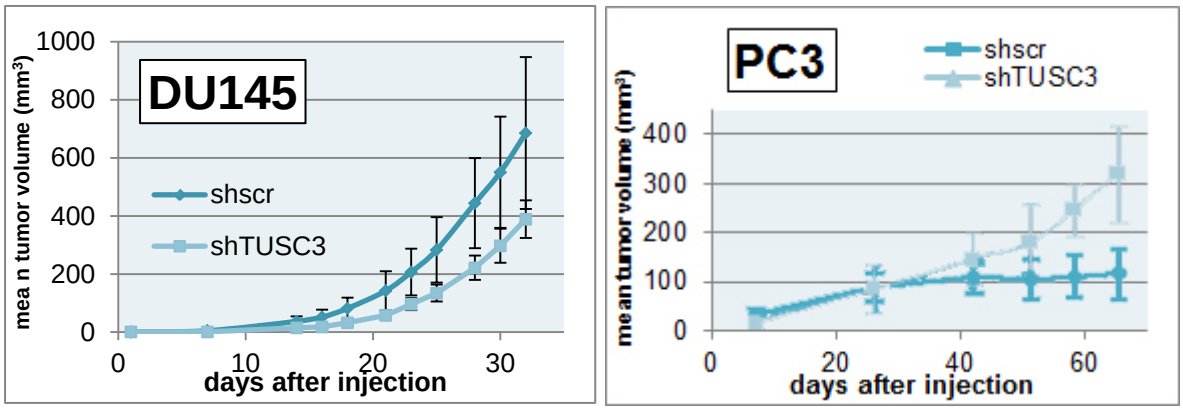

Figure 14: TUSC3 affects tumor size and growth rate in PC3 but not in DU145 xenografts. Control cell lines (shscr) were subcutaneously injected into the left flank while the silenced cell lines (shTUSC3) were injected into the right flank of athymic nude mice (n=8). Tumor growth was measured every three days until mice had to be sacrificed. Error bars represent the standard deviation of the mean (n=8). Tumors derived from DU145 cells were more rapidly growing than those from PC3 cells, but the former ones showed no significant difference in their growth rate. After approximately 50 days shTUS3 PC3 cells gained a growth advantage over their control counterparts. Overall, growth behavior in vivo mirrors data of cell viability in vitro obtained previously.

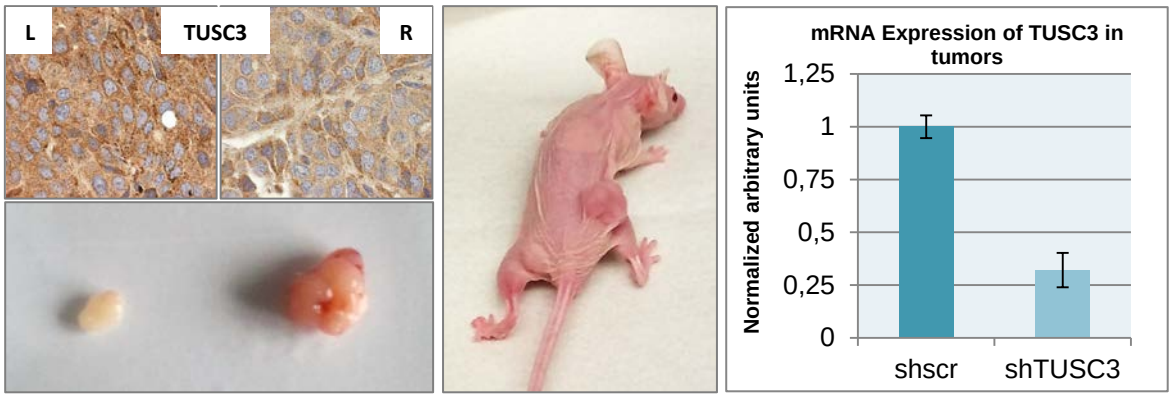

Figure 15: Analysis of tumors derived from xenografts. Upper left panel: shscr (L, left) and shTUSC3 (R, right) tumors were analyzed by immunohistochemistry with Anti-TUSC3 (abcam 65213, 1:300) antibody. Bottom left panel: Isolated tumors from the left flank (shscr) and the right flank (shTUSC3). Middle panel: athymic mice with growing tumors in the left flank (shscr) and the right flank (shTUSC3). Right panel: TUSC3 expression levels were determined by qRT-PCR analysis. Data was normalized to HPRT1 expression as housekeeping gene and shscr expression was set as one. Data from all tumors (n=8) were pooled and illustrated (right). Error bars represent the standard deviation of the mean.

3.1.4 TUSC3 silencing leads to increased AKT activation

We wanted to test, whether one of the most prominent signaling pathways in prostate cancer cells is altered to explain a possible increased viability. Given that both cell lines do not express the androgen receptor, we focused on the PI3K/AKT pathway. PI3K/AKT signaling triggers proliferation as well as survival. We determined signaling activation by detecting phosphorylation levels of AKT. We found only slight phosphorylation, ergo activation, of AKT in DU145 cells, which is explained by the fact that they express the phosphatase PTEN, a repressor of the PI3K/AKT pathway. Nevertheless, shTUSC3 cells of DU145 displayed more than the double amount of P-AKT if cultivated with 10% serum (Suppl. Data, Table 9). In case of PC3 cells, lacking PTEN (Vlietstra et al., 1998), we could observe a doubled increase in AKT phosphorylation when TUSC3 was silenced, independently of serum supplementation (Figure 16). But under serum starvation only approx. the half amount of P-AKT is detectable (Suppl. Data, Table 9). The difference in PTEN expression and the subsequent availability of AKT might explain the difference in viability we have observed in the two cell lines (see 3.1.2). Although we observed a more prominent effect in the absence of serum, we wondered, whether an upstream target of AKT was affected as well. Growth factor receptors are the major activators of the PI3K/AKT pathway, and we therefore studied EGFR and IGFR-1 as two prominent

members. Surprisingly, we found upregulation of EGFR only in DU145 cells, where viability was unaffected, while PC3 displayed very low EGFR levels (Figure 17). Another notable finding to point out is the observation, that EGFR expression was unaffected at the mRNA level (Suppl. Figure 2), suggesting a mechanism at the post-transcriptional and/or post-translational level. IGFR-1β expression was not affected in both prostate cancer cell lines upon TUSC3 silencing (Figure 17).

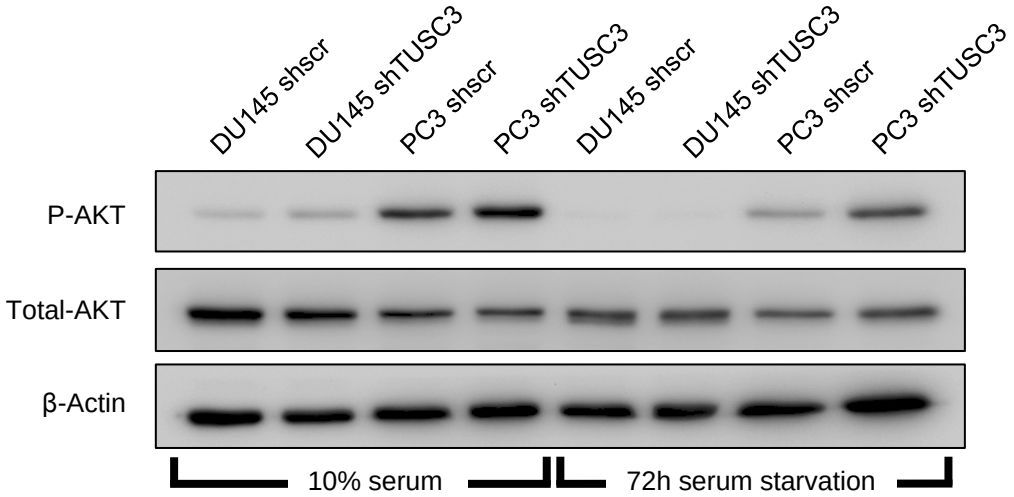

Figure 16: AKT phosphorylation is increased in silenced prostate cancer cell lines. Phosphorylation of AKT (P-AKT) is increased in shTUSC3 PC3 cell lines independent of the presence of serum. DU145 show only modest phosphorylation of AKT most likely due to PTEN expression and under serum starved conditions P-AKT was under the level of detection. The experiment was repeated three times and a representative immunoblot is shown. The quantitation of protein levels are given in the Supplemental Data (Table 9).

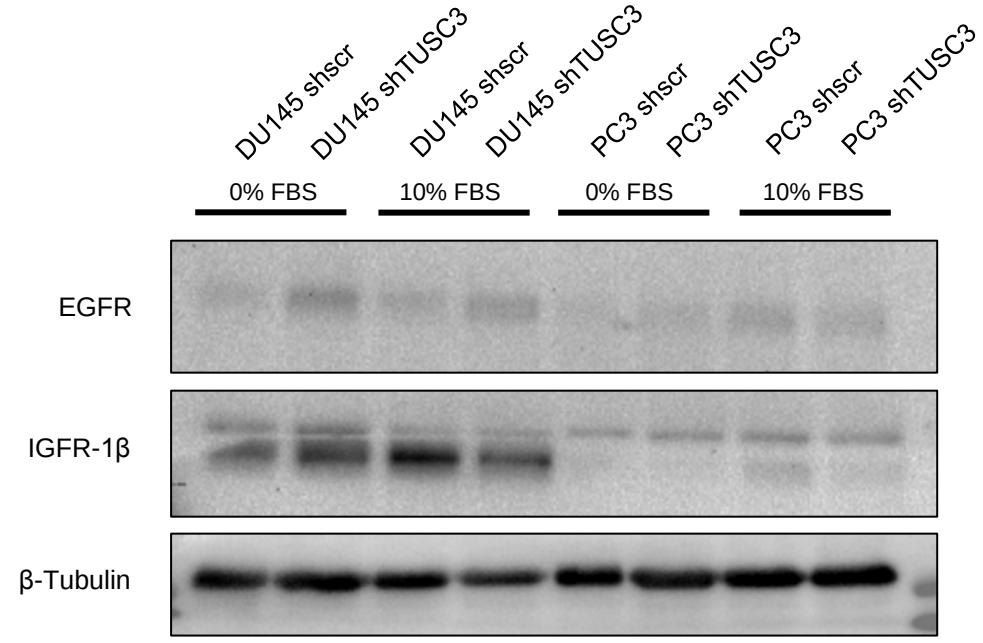

Figure 17: EGFR is differentially expressed in DU145 cells. EGFR protein levels are increased in shTUSC3 DU145 cells independent of serum conditions, while IGFR-1β protein levels remained unchanged. Detection of EGFR and IGFR-1β in PC3 cells was almost under the level of detection. The quantitation of protein levels are given in the Supplemental Data (Table 9).

3.1.5 EGFR inhibitors have no inhibitory effect on viability of prostate cancer cell lines

Inhibition of EGFR by small-molecule inhibitors has been recently discussed for the treatment of metastatic prostate cancer (Gallick et al., 2012). To inhibit EGFR phosphorylation and activation we treated shscr and shTUSC3 DU145 and PC3 cells, respectively, with two tyrosine kinase inhibitors, Lapatinib and Erlotinib. Both compounds are clinically implicated in cancer therapy – Lapatinib mainly in breast cancer (Higa & Abraham, 2007) and Erlotininb in non-small cell lung cancer and pancreatic cancer (Iyer & Bharthuar, 2010) – although, both are not yet approved by the FDA for prostate cancer treatment. Lapatinib and Erlotinib had no significant inhibitory effects on cell viability of both cell lines depending on TUSC3 expression, suggesting that neither EGFR (ERBB1) nor Her2/neu (ERBB2) is responsible for TUSC3 mediated AKT activation in these cells. Increased resistance of PC3 cells to Erlotinib treatment can be explained by their PTEN status, as this effect has been also described for lung cancer cells with PTEN loss (Sos et al., 2009).

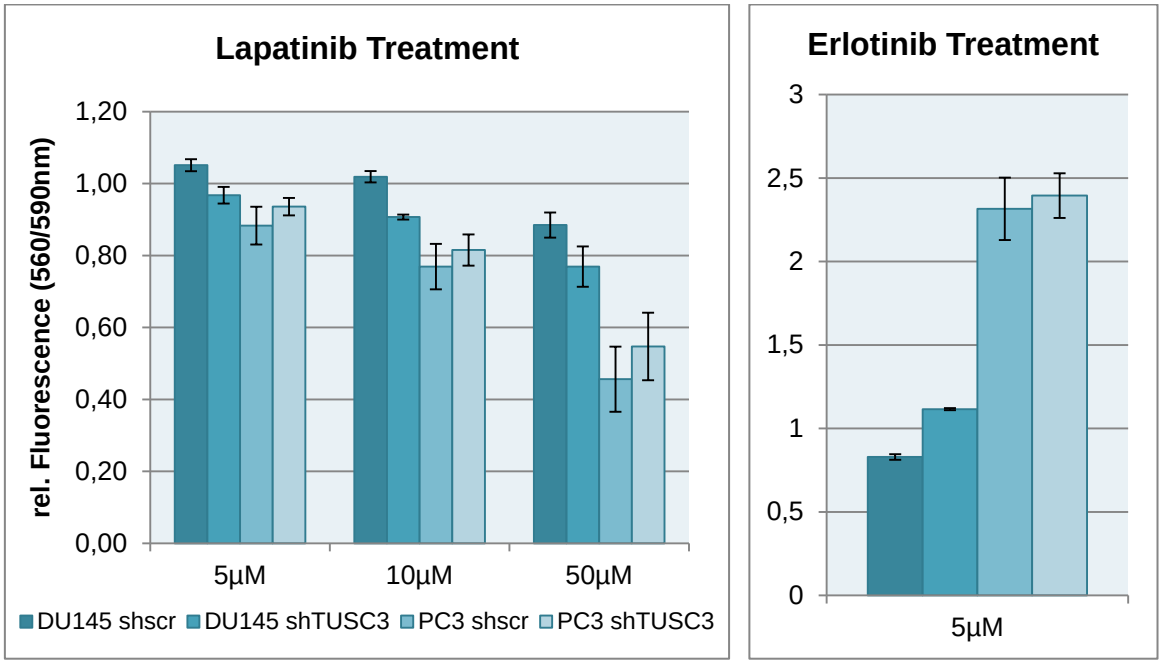

Figure 18: Treatment of prostate cancer cell lines with Lapatinib and Erlotinib for 72 hours. Cells were incubated in medium containing the compound or DMSO. After 72h Cell Titer Blue Reagent was added and fluorescence was measured. Cell numbers were normalized to DMSO controls of each cell line. Error bars represent the standard deviation of the mean (n=3). Increasing amounts of Lapatinib reduce cell viability in DU145 and PC3 cells independent of TUSC3, whereas Erlotinib treatment strongly affected DU145, but not PC3 cells.

3.1.6 Silencing of TUSC3 affects migration and invasion of PCa cell lines

Next we addressed the question, whether TUSC3 affects migration and invasion. Both cell properties are required for a metastatic behavior of cancer cells and define the aggressiveness of a tumor. To study migration we performed a scratch assay and analyzed wound closure for several days. Cells were treated with mitomycin c to inhibit cellular proliferation and to monitor only migration. We observed that TUSC3 silenced cells show a higher migratory potential compared to shscr cells indicated by faster wound healing (Figure 19). Additionally, we followed invasion through Matrigel, whose components imitate the extracellular matrix and migration through a basement membrane with a pore-size of 8µm. We found that cells with lower TUSC3 expression display enhanced invasiveness compared to control cells (Figure 20).

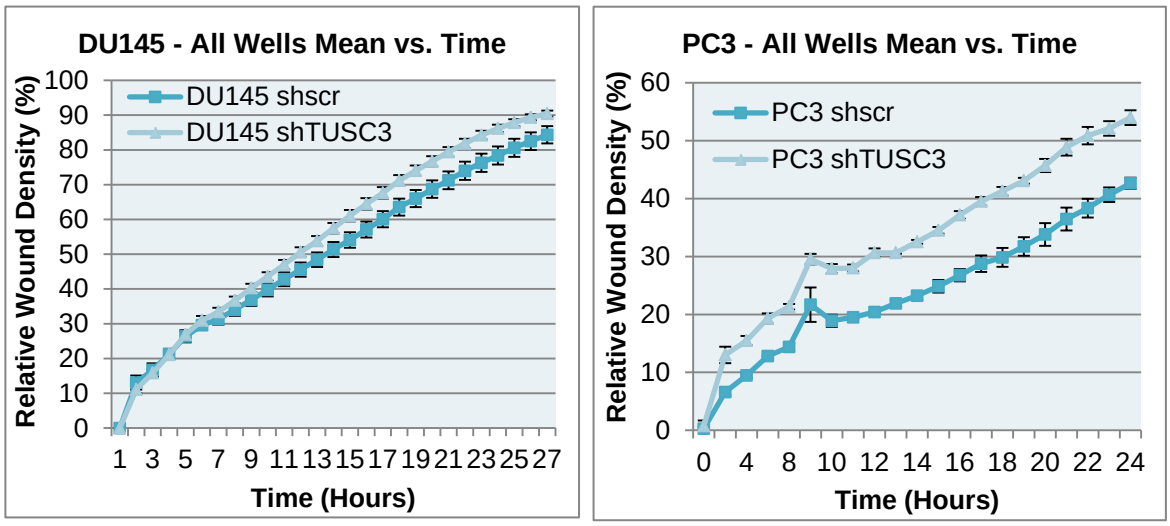

Figure 20 TUSC3 silenced prostate cancer cell lines showed increased migration. Wounds were scratched using a 96-well Wound Maker. Wound closure was followed for 30 hours by the IncuCyte ZOOM system taking images every 60 minutes, and representative images are shown on pages 55 and 56. Statistical analysis was calculated from 16 replicates in case of DU145 and 3 replicates of PC3 cells, shscr and shTUSC3, respectively. Error bars represent the standard deviation of the mean. After 23 hours the relative wound confluence was approximately 10% denser in case of shTUSC3 in both cell lines.

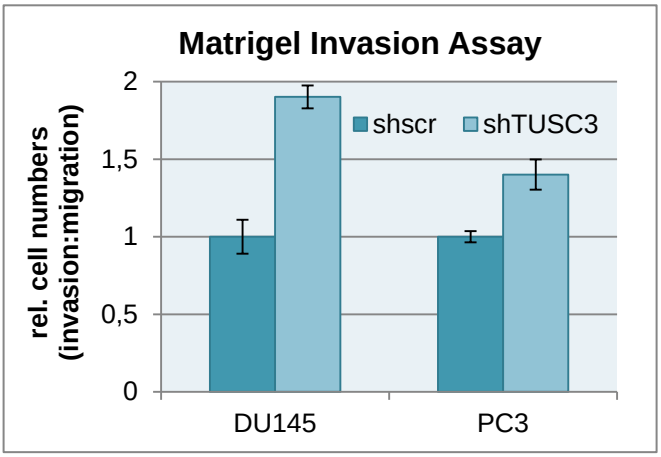

Figure 19: TUSC3 silenced prostate cancer cell lines showed increased invasion. DU145 and PC3 shTUSC3 cells and respective controls were seeded in triplicates on Matrigel-coated Boyden chambers in 24-well plates. The lower chamber contained 20% fetal bovine serum as chemoattractant. After 18h of incubation cells were fixed with 10% Formalin, stained with 0.05% crystal violet and counted under a light microscope. Control cells were plated onto uncoated plates to monitor migration and standardize cell numbers. Error bars represent the standard deviation of the mean (n=3).

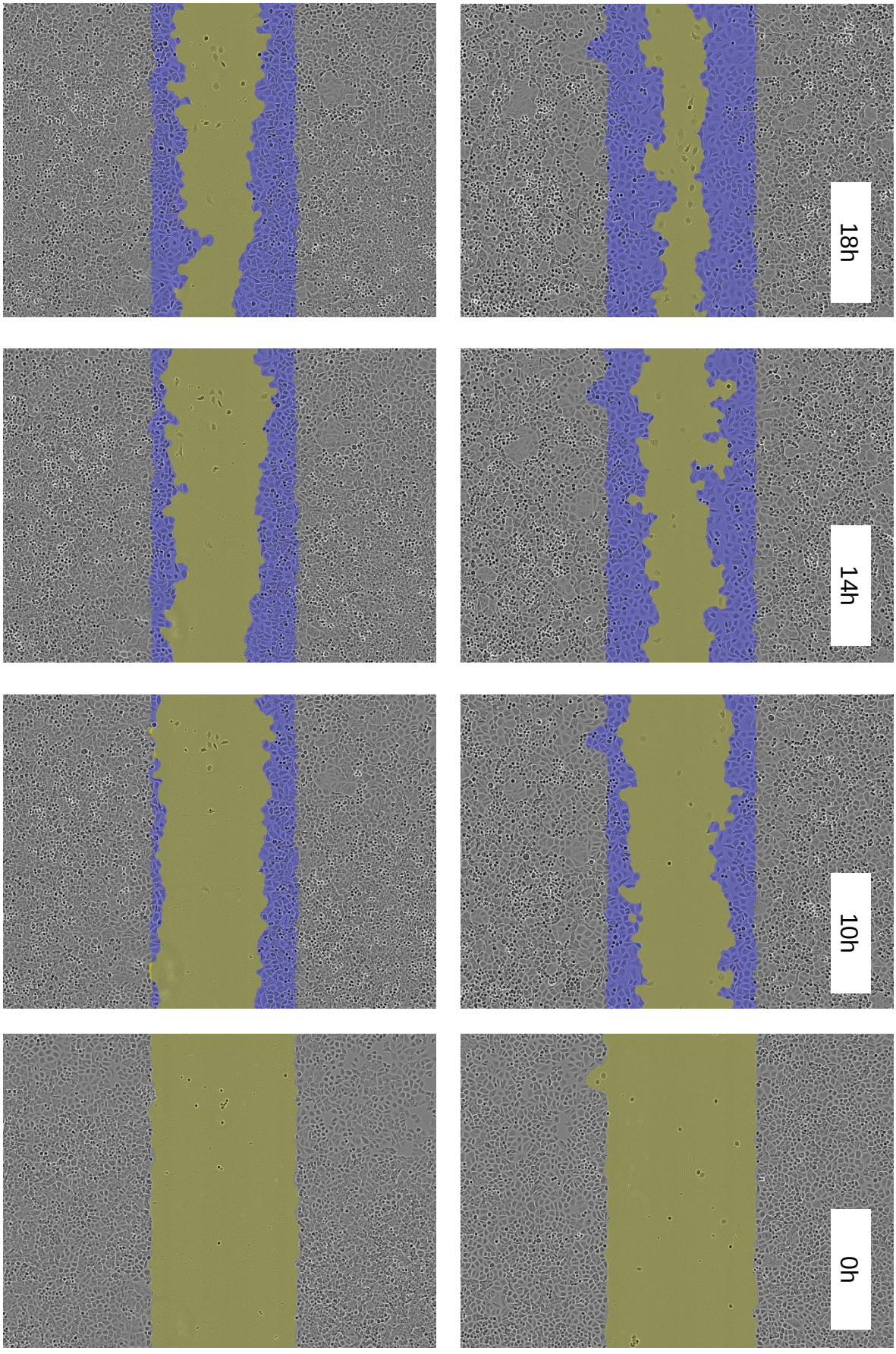

DU shscr DU shTUSC3

(legend on previous page)

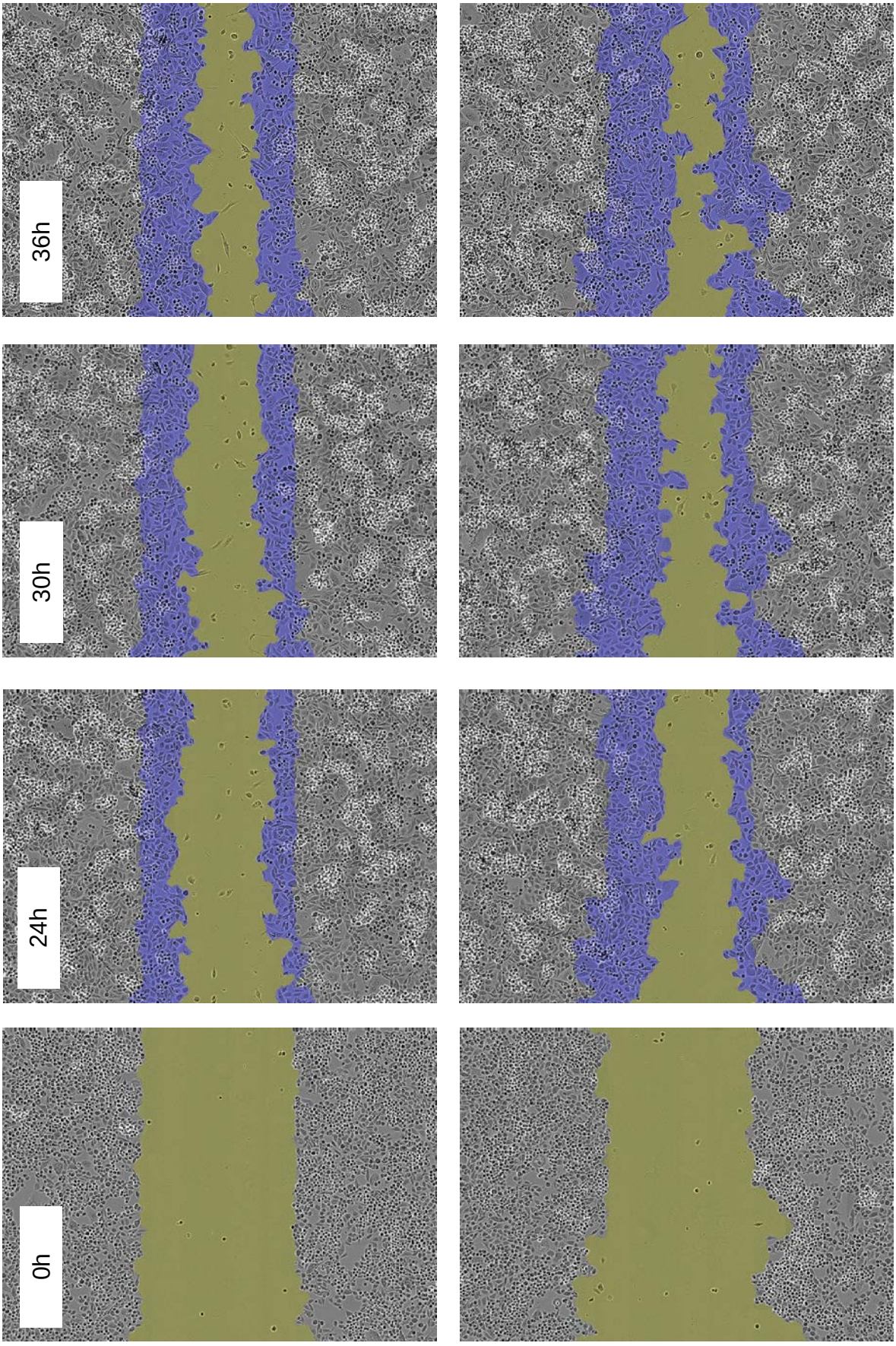

PC3 shscr PC3 shTUSC3

(legend on page 56)

3.1.7 E-Cadherin and CD44 but not Integrin-β1 expression is affected by TUSC3

An increase of the invasion potential in cancer cells is often linked to alterations in the expression of adhesion molecules (Cavallaro & Christofori, 2001). Therefore, we analyzed the protein levels of E-Cadherin, Integrin-β_1, and CD44 by immunoblotting. Interestingly, E-cadherin highly accumulated in DU145 cells with lower TUSC3 expression, while its expression was widely unaffected in PC3 cells independent of serum conditions. Furthermore, Integrin-β_1 expression was not affected by TUSC3 in both cell lines (Figure 21). Contrary to E-cadherin, expression of CD44 was significantly lower in shTUSC3 PC3 cells, while we were not able to detect it in DU145 cells at all (Figure 22).

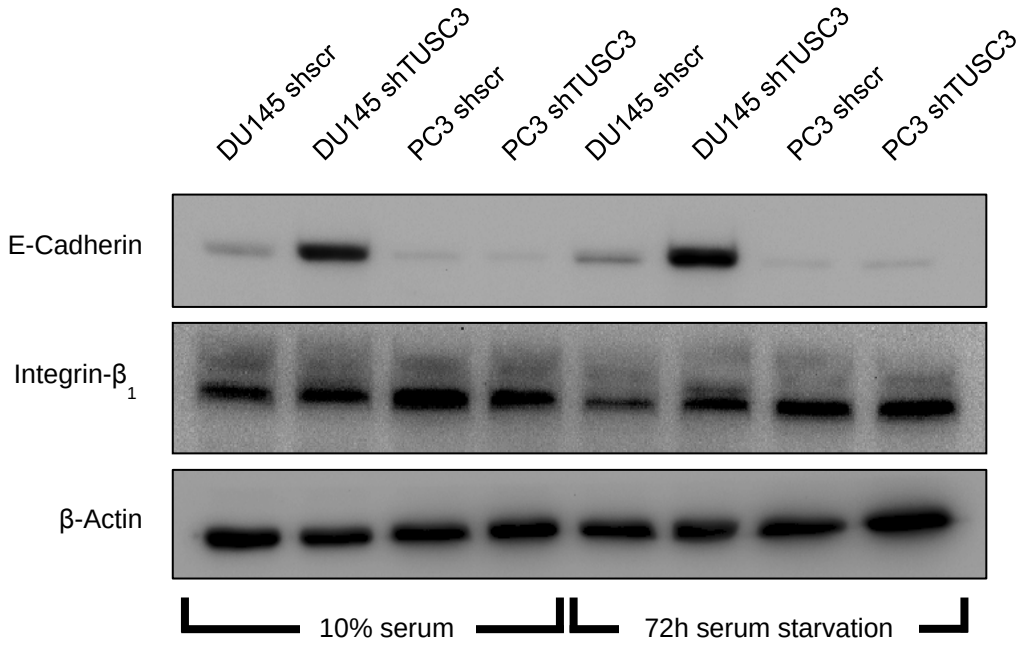

Figure 21: E-cadherin and Integrin-β1 protein levels in prostate cancer cell lines. E-cadherin is almost under the level of detection in the PC3 cell line. In DU145 cells E-cadherin is expressed independent of serum conditions, but accumulates in shTUSC3 cells compared to respective control cells. Integrin-β_1 is not affected by TUSC3 or serum conditions in both cell lines. The quantitation of protein levels are given in the Supplemental Data (Table 9).

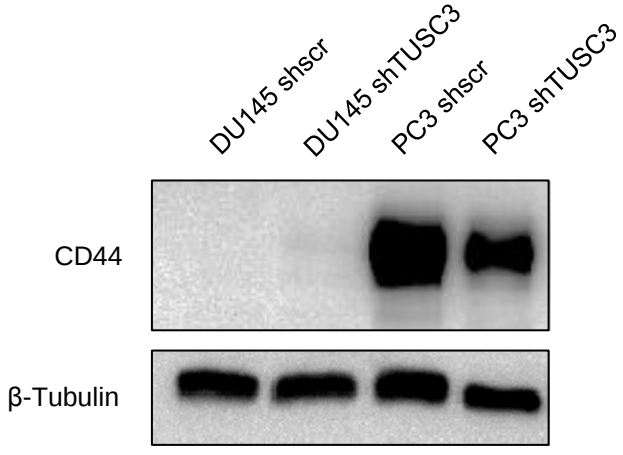

Figure 22: Protein levels of CD44 in prostate cancer cell lines. While we were not able to detect CD44 protein expression in DU145 cells at all, shTUSC3 PC3 cells are showing lower expression compared to shscr cells.

3.2 Functionality

3.2.1 TUSC3 is present in the endoplasmic reticulum and is part of the oligosaccharyltransferase complex

In silico prediction revealed close homology of TUSC3 to a yeast subunit of the oligosaccharyltransferase, a multienzymatic complex, involved in N-glycosylation (Kelleher & Gilmore, 2006). In eukaryotes, this process takes place exclusively in the ER. We used fluorescence microscopy to identify in which cellular compartment TUSC3 is expressed. We stained the ER using a commercially available plasmid expressing the ER-resident protein calreticulin. We cloned the TUSC3 cDNA into a vector containing an EGFP tag to obtain TUSC3-EGFP expression. DU145 cells were transfected with both plasmids and nuclei were stained with DAPI. Fluorescence images revealed a wide overlay of the TUSC3 and the ER signals, though it cannot be excluded that TUSC3 is also expressed in other compartments of the cell as well. The ER is a highly dynamic organelle and constantly interacting with the Golgi apparatus. Therefore, it could be possible that TUSC3 is temporarily located at this site too (Figure 23).

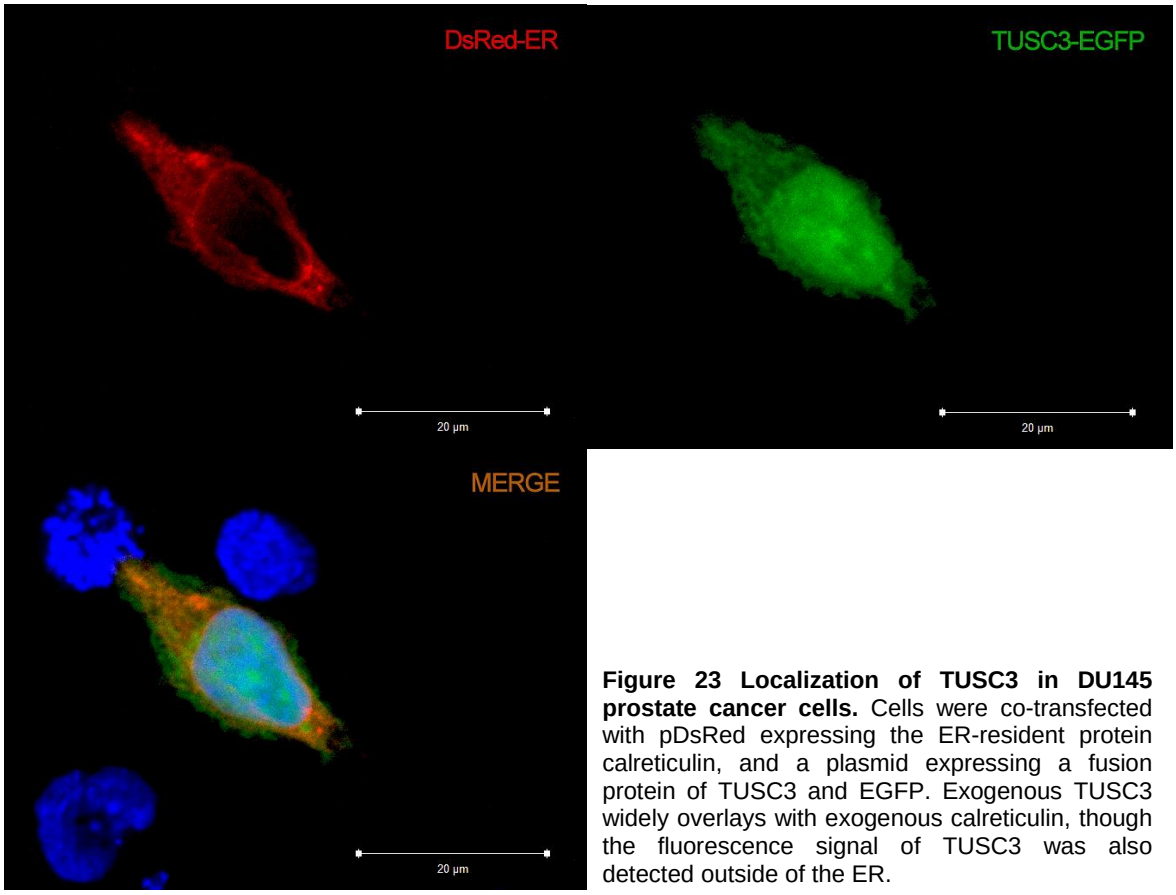

Figure 23 Localization of TUSC3 in DU145 prostate cancer cells. Cells were co-transfected with pDsRed expressing the ER-resident protein calreticulin, and a plasmid expressing a fusion protein of TUSC3 and EGFP. Exogenous TUSC3 widely overlays with exogenous calreticulin, though the fluorescence signal of TUSC3 was also detected outside of the ER.

Additionally, we overexpressed TUSC3 in HEK293 cells and performed immunoprecipitation against STT3A and STT3B, the catalytic subunits of the oligosaccharyltransferase complex. We found that TUSC3 and STT3B precipitate in both directions, suggesting a physical interaction of these subunits in mammalian cells (Figure 24). However, we were unable to find an interaction between TUSC3 and STT3A (Suppl. Figure 3). Taken together, these results support a putative role of TUSC3 in N-glycosylation.

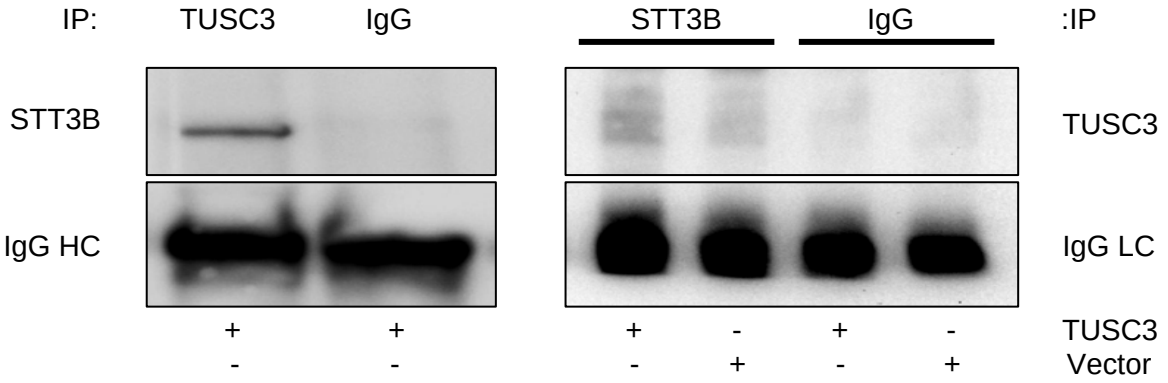

Figure 24: Co-Immunoprecipitation of STT3B and TUSC3 revealed physical interaction of both OST subunits in mammalian cells. HEK293 cells were transiently transfected with a TUSC3 expressing vector. TUSC3 was precipitated with 2µg of antibodies against STT3B or STT3A, respectively vice versa. While immunoprecipitaion with STT3A failed (Suppl. Figure 3), we could precipitate the other two subunits in both directions.

3.2.2 No detectable changes in overall glycosylation upon TUSC3 silencing

To get a rough idea of the overall protein N-glycosylation in our prostate cancer cell lines, we stained total protein lysates with two commercially available lectins. These plant-derived proteins detect specifically glycoproteins, in case of Concanavalin A (ConA), glycoproteins carrying α-D-mannoses and α-D-glucoses, and in case of Phytohemagglutinin (PHA-L), glycoproteins with oligosaccharides containing galactose, N-acetylglucosamine, and mannose. With this approach, we were not able to observe distinct differences in the glycoprotein pattern of both cell lines and their variants by immunoblotting (Figure 25). Moreover, when we used ConA to stain the entire cells followed by immunocytochemistry, we were not able to detect differences in their glycosylation staining patterns (Figure 26). It should be noted that subtle changes in N-glycosylation and/or changes affecting only one or a few glycoprotein(s) might not be able

to detect by this method.

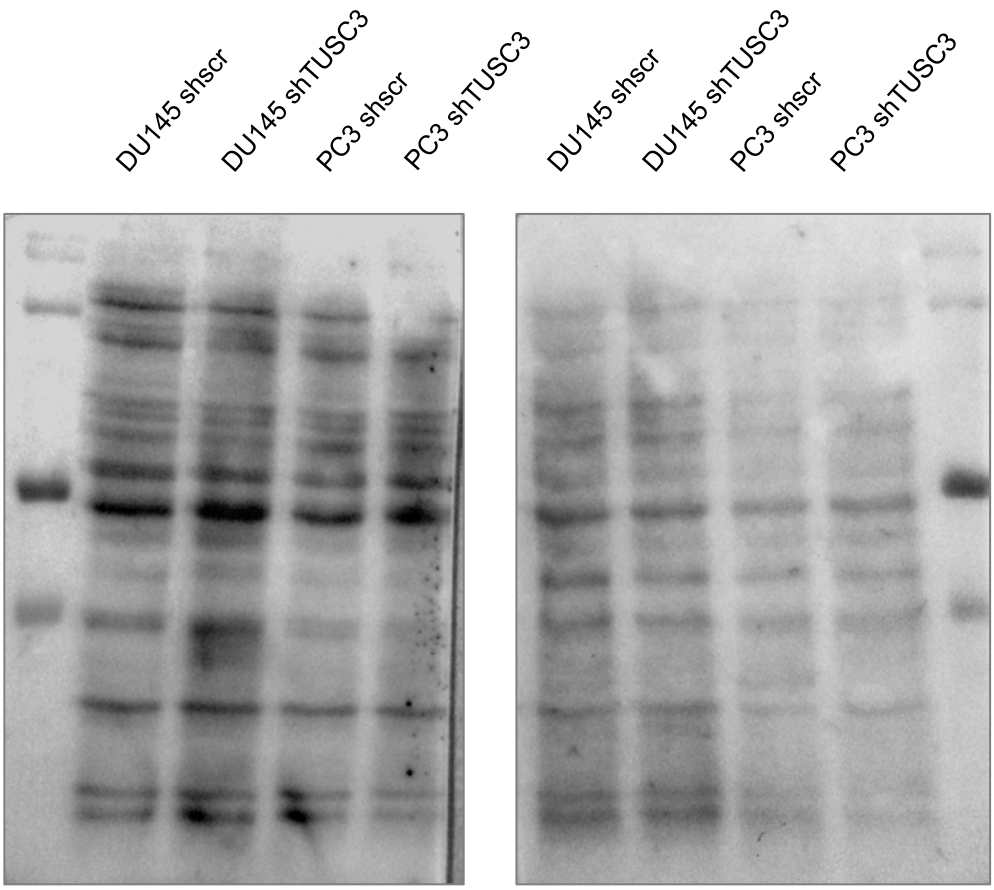

Figure 25: Eastern Blots are showing equal overall glycoprotein patterns. Total protein lysates were separated on a 10% polyacrylamide gel and blotted onto PVDF-membranes. Membranes were blocked in PBS/Tween (0.5%) for Concanavalin A (1µg/ml) and with 1% BSA/PBS for PHA-L (2µg/mL). Lectin incubation took place 2 hours in blocking buffer at room temperature.

Furthermore, we have used another approach first introduced by Contessa and his colleagues (Contessa et al., 2010). They were using luciferase, an enzyme from fireflies, to measure glycosylation *in vitro*. Luciferase (Luc) is carrying three potential glycosylation sites which are unused *in vivo*, since the native protein does not enter the ER. Therefore, the ER targeting sequence from EGFR was fused with the luciferase gene (E-Luc). It is assumed that glycosylation of E-Luc inhibits its function (Contessa et al., 2010). We stably transfected our prostate cancer cell lines with an expression vector carrying the E-Luc cDNA or the empty vector (pcDNA3.1+), serving as negative control, and measured luminescence as an indication for luciferase activity. We found a 5 to 10 fold increase of luminescence in case of TUSC3 silenced cells (Figure 27), suggesting that N-glycosylation might be affected in these cells.

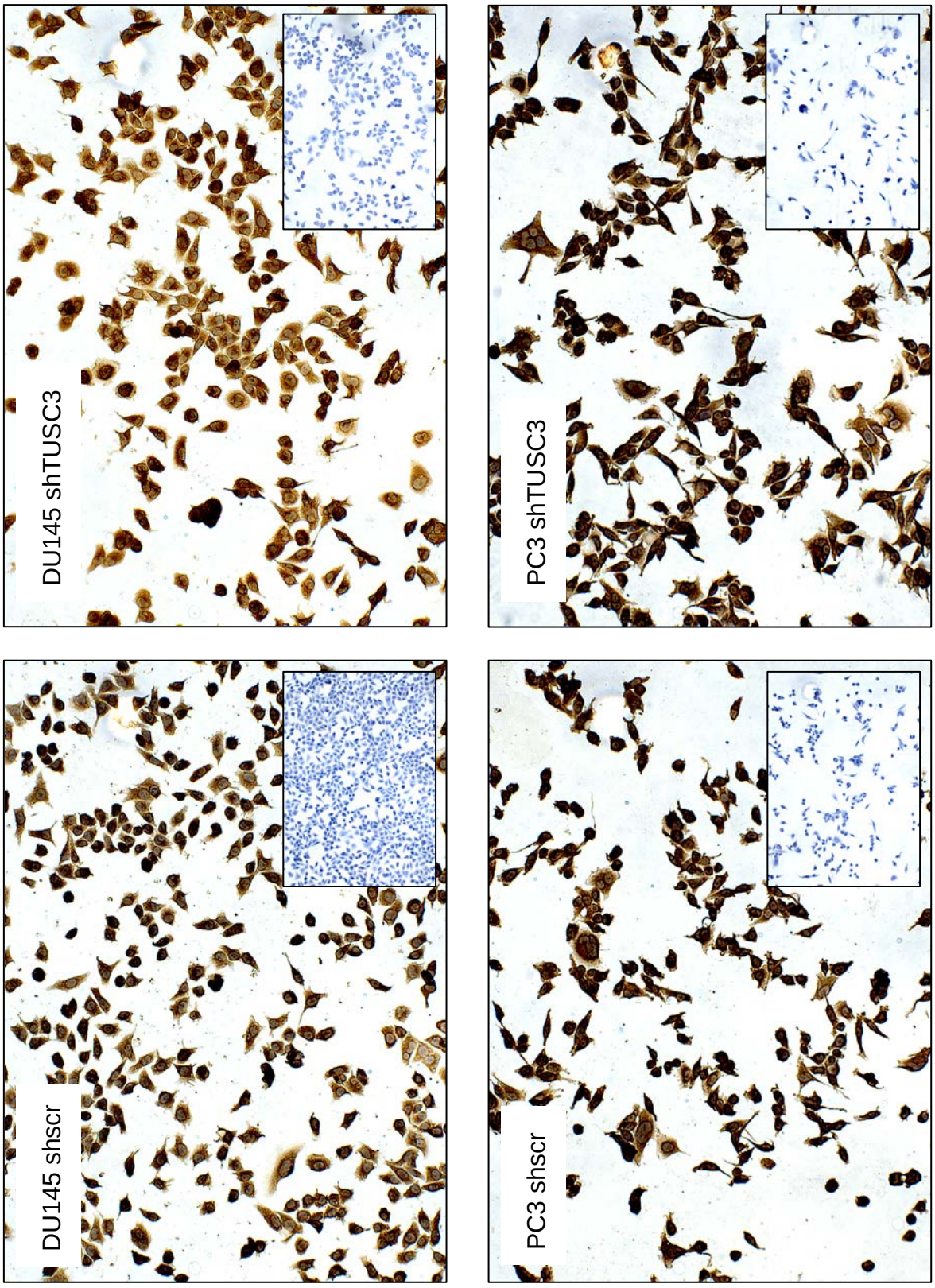

Figure 26: Lectin-based Immunocytochemistry. Cells were grown on chamber slides until reaching 70% confluency. After washing the cells with PBS, they were fixed with 10% formalin, washed, permeabilized with 0,1% Triton-X/PBS and washed again. Cells were blocked in 5% BSA for 30 minutes and incubated with Concanavalin A (ConA-HRP) for 2 hours at 4°C. After six washing steps with 1x PBS/Tween, visualization was realized by incubation with 3,3-diaminobenzidine-(DAB) hydrogen peroxide for 30 seconds at room temperature. Slides were rinsed in distilled water, counterstained with haematoxylin, rinsed again in water and dehydrated in a graded alcohol series. The slides were mounted, covered with cover slips, and analyzed under a light microscope. Insets are showing negative controls with haematoxylin staining only.

Nevertheless, when we were detecting luciferase levels by immunoblotting, we found a stronger signal of the enzyme in the TUSC3 silenced cells as well. Therefore, we cannot exclude that instead of glycosylation being affected, differences in transfection efficiency may be responsible for the different luminescence signal intensities observed. Another aspect that supports this assumption is provided by an *in vitro* deglycosylation experiment (Figure 27). When we were treating the protein lysate with a glycosidase (PNGase F), we observed a band shift of E-Luc, confirming that E-Luc is indeed glycosylated. Without prior treatment, we were not able to see the band shift in cells with silenced TUSC3, suggesting that TUSC3 does not contribute to hypoglycosylation.

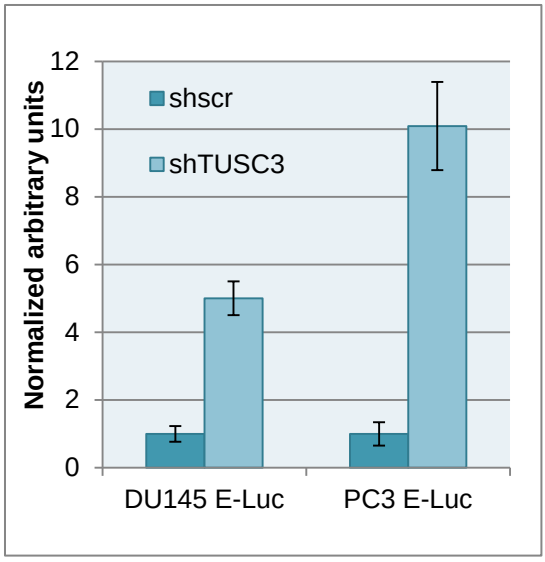

Figure 27: Luciferase assay to measure N-glycosylation efficiency in prostate cancer cells. Cells were stably transfected with E-Luciferase or the empty vector by using FuGene 6 reagent (n=3). Luminescence was measured on a multimode microplate reader. Luminescence signal was 5 to 10 times higher in shTUSC3 cells compared to control cells. **Protein levels of Luc and E-Luc, detected by Immunoblotting (underneath).** A representative Immunoblot with DU145 transfectants is shown. Protein lysates were prepared from cells and 20µg were treated with PNGase F according to manufacturer's instructions. Proteins were separated on a 10% polyacrylamide gel and blotted onto a PVDF membrane followed by overnight incubation of anti-Luciferase (1:5000) and anti-actin (1:1000) antibody. The band corresponding to E-Luc shows higher electrophoretic mobility, indicating deglycosylation by PNGase F. The band shift is not visible in shTUSC3 cells without PNGase F treatment. The Luc protein band is unaffected upon glycosidase treatment.

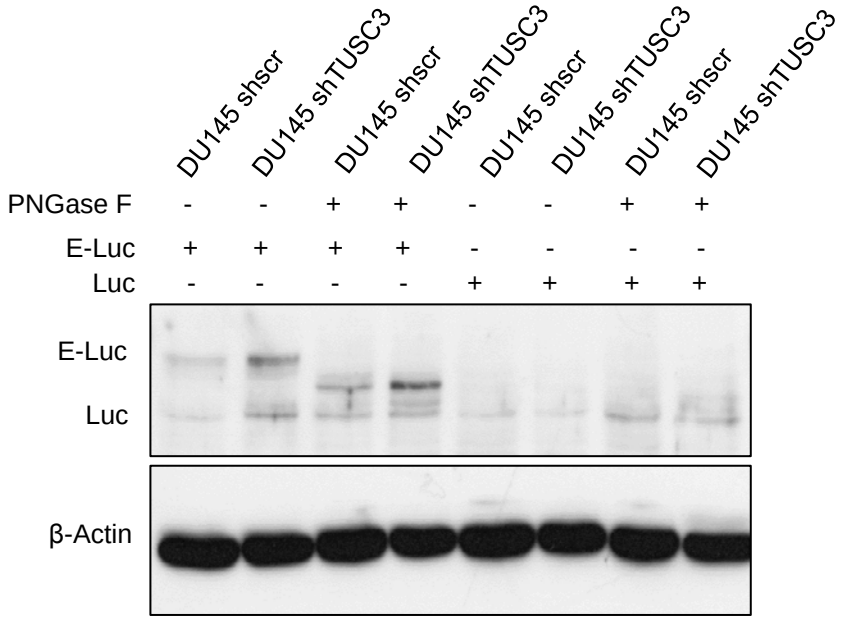

3.2.3 Silencing of TUSC3 elevates ER stress

It is well known that impaired N-glycosylation affects glycoprotein folding and dysregulation of this process may result in ER stress. Therefore, we addressed the question, whether TUSC3 loss mediates an ER stress response in prostate cancer cell lines. We induced ER stress by blocking N-glycosylation after treatment of cells with tunicamycin, thus causing the accumulation of unfolded proteins. DU145 cells display only a slight difference referring to TUSC3 expression upon tunicamycin treatment, however, viability was strongly reduced compared to PC3 cells. Furthermore, shTUSC3 PC3 cells showed increased resistance to tunicamycin after 72 hours of treatment compared to control cells (Figure 28). Next, we studied molecular markers indicating ER stress. We analyzed C/EBP homology protein (CHOP), an inducer of apoptosis (Szegezdi et al., 2006), and X-box binding protein 1 (XBP-1). We observed that induction of CHOP is reduced in PC3 cells with lower TUSC3 expression, indicating less ER stress signaling. Furthermore, we found stronger expression of unspliced XBP-1 mRNA in TUSC3 silenced cells and thus higher ratios of the spliced/unspliced mRNA in shscr cells of both cell lines (Figure 29), indicating enhanced splicing (Davies et al., 2008) and therefore ER stress response when TUSC3 was down-regulated.

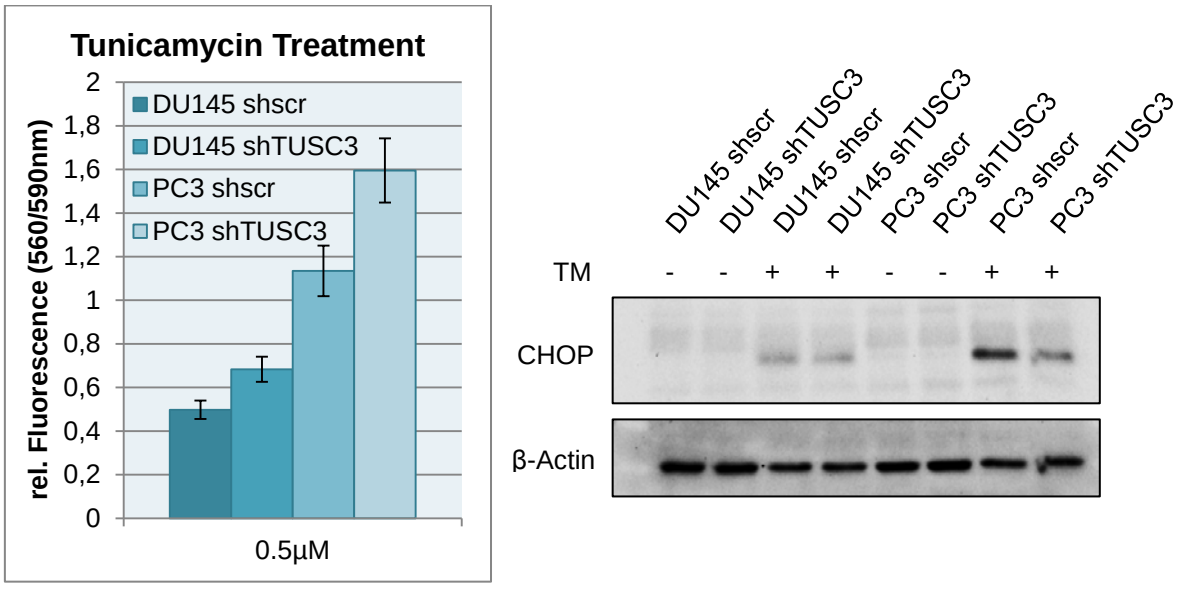

Figure 28: Knockdown of TUSC3 increases the resistance of PC3 cells to tunicamycin (left). Cells were incubated in medium containing 0.5µM tunicamycin or DMSO. After 72h Cell Titer Blue Reagent was added and fluorescence was measured. Cell numbers were normalized to DMSO controls of each cell line. Error bars represent the standard deviation of the mean (n=3). **Induction of CHOP by tunicamycin treatment is markedly reduced in shTUSC3 PC3 cells (right).** Cells were incubated for 18 hours in the presence of 0.5µM tunicamycin (TM). Afterwards, proteins were isolated and analyzed by immunoblotting using Anti-CHOP (1:500) and Anti-actin (1:1000) antibodies.

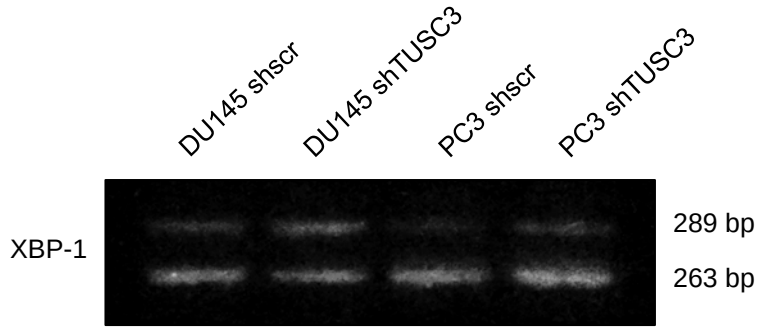

	DU145 shscr	DU145 shTUSC3	PC3 shscr	PC3 shTUSC3
289bp	5,80	7,66	4,72	6,0
263bp	9,66	8,68	13,43	14,58
Ratio	1,67	1,13	2,85	2,43

Figure 29: The amount of unspliced XBP-1 mRNA is higher in TUSC3 silenced prostate cancer cell lines. Cells were treated with 5µM tunicamycin for 18 hours and RNA was isolated afterwards. After reverse transcription into cDNA, expression levels of XBP1 mRNA were measured by semi-quantitative PCR. Intensity of the bands was quantified using ImageJ software (Rasband, W.S., ImageJ, U. S. National Institutes of Health, Bethesda, Maryland, USA, http://imagej.nih.gov/ij/, 1997-2012) and the ratio of spliced (263 bp) to unspliced (289 bp) isoforms was calculated.

4 Discussion

One of the most frequent cytogenetic alterations in prostate cancer is the deletion of the short arm of chromosome 8, which is associated with poor prognosis as it often occurs during tumor progression (El Gammal et al., 2010). A study from Cher and colleagues detected a loss of 8p22 in 80% of prostate cancer lymph node metastases (Cher et al., 1996). Many other studies focused on the clinical significance of 8p loss and its role in predicting pathological staging (Matsuyama et al., 2003; Nakano et al., 2008; Troutman et al., 2010). Despite the extensive and long lasting observations, neither the mechanism responsible for 8p loss nor a specific tumor suppressor gene (TSG) has been identified yet. Pils and colleagues were the first who systematically screened 8p22 for potential TSG candidates, identifying two genes, TUSC3 and EFA6R, with impact on survival in ovarian cancer (Pils et al., 2005). Later they have suggested that hypermethylation of TUSC3 is a prognostic factor in ovarian cancer (Pils et al., 2013). So far, alterations of TUSC3 expression had been only associated with diseases described as congenital disorders of glycosylation (CDGs), e.g., mental retardation (Loddo et al., 2013; Mhamdi et al., 2011). In the present work, we present first evidence that TUSC3 cooperates to suppress tumorigenesis in prostate cancer as well.

By silencing TUSC3, we showed an increase of cellular viability of PTEN negative prostate cancer cells *in vitro* and *in vivo*. Moreover, we found that TUSC3 loss contributes to enhanced migration and invasion of prostate cancer cells *in vitro*, which was independent on PTEN expression. We further showed that increased activation of the PI3K/AKT pathway through AKT phosphorylation might contribute to increased viability of prostate cancer cells lacking PTEN, a genetic status commonly found in prostate cancer patients. The mechanism leading to AKT activation due to TUSC3 loss remains to be further investigated. In addition to changes in AKT activation, two adhesion molecules (E-cadherin and CD44, respectively) were differentially affected upon TUSC3 silencing, again, depending on the PTEN status of the PCa cell line. PCa cell line DU145 showed increased expression of E-cadherin and enhanced migratory potential in case of silenced

TUSC3 expression. This is conflicting with previous observations showing that high expression of E-cadherin is associated with decreased migration (Chen et al., 1997). Moreover, E-cadherin acts as a suppressor of metastasis and its proper function is dependent on N-glycosylation (Zhao et al., 2008). Therefore, it seems likely that even if E-cadherin accumulates in cells, it cannot fulfill its function due to deficient post-translational mechanisms. Furthermore, both prostate cancer cell lines I used in this study were derived from metastases, bone in case of PC3 (Kaighn et al., 1979) and brain in case of DU145 (Stone et al., 1978). Therefore, a lower expression of E-cadherin can be assumed a priori. More interestingly in this sense is the re-expression of E-cadherin in these metastatic cells by TUSC3 silencing. To settle in a new environment, a metastatic cell needs to re-activate E-cadherin, which suggests loss of 8p and TUSC3 as a late event in tumor progression and a selective advantage for these cells to form metastases in distant organs (Bae et al., 2011). CD44, another glycoprotein, has been identified as a metastasis suppressor gene in prostate cancer (Gao et al., 1997). It is repressed in PC3 cells with lower TUSC3 expression and is confirmed by increased invasion potential of these cells.

Overall, we found that TUSC3 influences the migratory and invasion potential of prostate cancer cells by changing the expression of adhesion molecules dependent on the heterogenous cellular background of DU145 and PC3 cell lines. Moreover, our work is supported by recent findings of Vanhara and colleagues demonstrating that loss of TUSC3 influences proliferation, migration, and invasion in ovarian cancer (Vanhara et al., 2013).

To get an idea how TUSC3 is involved in these processes we decided to study its function on the molecular level. Amino acid sequence comparison revealed close homology of TUSC3 to Ost3p in yeast, which is involved in protein N-glycosylation (Kelleher et al., 2003). This post-translational modification supports proper protein folding and therefore its function. We confirmed physical interaction of TUSC3 with the catalytic subunit of the mammalian OST enzyme complex subunit STT3B and its localization inside the ER, where N-glycosylation occurs in mammalian cells. Similar findings in ovarian cancer cells

have been previously obtained by others as well (Vanhara et al., 2013). This includes an interaction of TUSC3 with STT3A, another isoform of the OST catalytic subunit, which we could not observe, for reasons that remain unclear so far. Loss of Ost3p leads to severe hypoglycosylation of selected targets in yeast (Karaoglu et al., 1995). Altered N-glycosylation might contribute to the cellular effects we present in this work; however, firm evidence of a link between N-glycosylation and the development and metastasizing of prostate cancer is still missing. Identification of (a) specific glycoprotein(s) that is (are) affected by TUSC3 silencing proved to be difficult due to the limited methods available and the plethora of possible targets. By SDS-PAGE, proteins are separated according to their molecular weight, which is influenced by protein modifications. Differential migration of glycosylated proteins compared to their unglycosylated variants can be shown by glycosidase treatment prior to separation. The resulting characteristic shift without treatment could not be observed in case of any target displayed by this method when comparing control and TUSC3 silenced cell lines which would indicate apparent functional glycosylation. Detection of glycoproteins with two different lectins revealed no distinguishable difference in both PCa cell lines and their TUSC3-silenced counterparts as well. It has to be considered that more sensitive methods, e.g. mass spectrometry analysis, are required to show differences in protein modifications in consequence of TUSC3 loss, which might be only of qualitative rather than quantitative nature as proposed for Ost3p in yeast (Schulz et al., 2009).

Additionally, we observed that PC3 cells with less TUSC3 expression are more resistant to tunicamycin treatment, a compound which induces ER stress by inhibition of N-glycosylation (Bull & Thiede, 2012). Furthermore, the transcription factor CHOP, an inducer of apoptosis through ER stress (Teske et al., 2013) was downregulated in TUSC3-silenced PC3 cells. The increase in AKT activation might contribute to these effects as well. It has been shown that active AKT promotes glucose uptake by promoting the translocation of the GLUT-4 glucose transporter to the cell membrane (Summers et al., 1998). An increased glucose uptake positively affects N-glycosylation and antagonizes

ER stress. Recently, a crosstalk between ER stress response and AKT activation through GRP78/BiP has been demonstrated in prostate cancer pathogenesis (Fu et al., 2008).

So far, only one publication has been dealing with the function of TUSC3 and its paralogue MagT1, assigning them to a role in magnesium transport (Zhou & Clapham, 2009). In the present study, we propose alternative functions of TUSC3, considering previous *in silico* prediction and analysis of its subcellular localization. The data we obtained regarding ER stress response are demanding further investigations, especially since currently a number of anticancer drugs targeting the unfolded protein response are in development (Suh et al., 2012).

Future studies should focus also on the glycosylation status of membrane-bound growth factor receptors, which are known targets of N-glycosylation and are involved in the PI3K/AKT pathway. Additionally, glycosylation is involved in biological processes such as intercellular or cell-matrix interactions (Helenius & Aebi, 2001). Thus, adhesion molecules, e.g., E-cadherin, display targets as well and might be responsible for cancer initiation and progression with regard to TUSC3 loss. Moreover, a possible involvement of TUSC3 in ER stress might enclose a newly emerging field in oncology. The effects observed in this study were achieved by silencing TUSC3 and we are aware of the fact that the remaining activity might compensate more dramatic effects that would be caused by a complete loss as found in tumors. The loss of TUSC3 might provide the cell with advantages necessary to compete in the tumor microenvironment. It is well accepted that Darwinian processes inside a tumor select for cells with such advantages and drive tumor progression, as we showed for TUSC3 *in vivo* using xenograft models.

In summary, the present work provides first evidence that loss of TUSC3 promotes tumorigenicity of prostate cancer cells *in vitro* and affects tumor growth *in vivo*. Our findings contribute to a better understanding of the so far poorly described putative TSG by introducing plausible explanations which stimulates further studies.

5 Supplemental Data

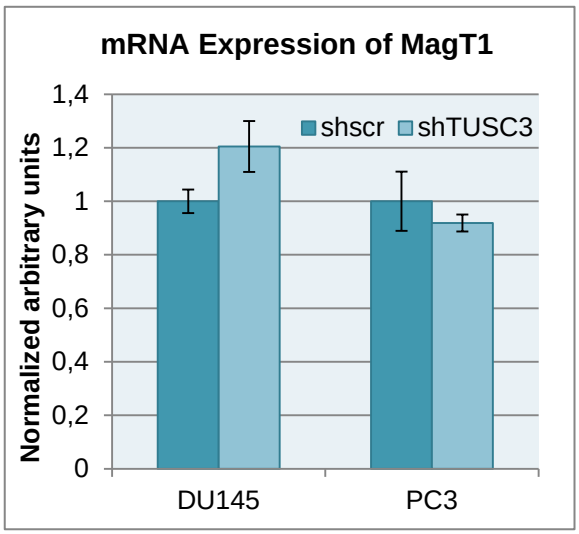

Supplementary Figure 1 (referring to 3.1.1): Expression of MagT1 remains essentially unaffected upon TUSC3 silencing. MagT1 mRNA expression was measured by qRT-PCR. Data was normalized to HPRT1 expression as housekeeping gene, while MagT1 expression in shscr cells was set as one. Error bars represent the standard deviation of the mean (n=3). shRNA targeting TUSC3 is not significantly affecting MagT1 expression, a TUSC3 paralogue in human, located at the X-chromosome.

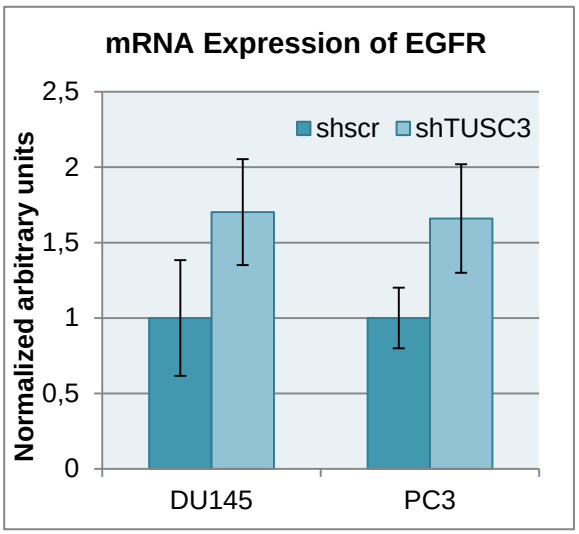

Supplementary Figure 2 (referring to 3.1.4): mRNA levels of EGFR are not significantly different after downregulation of TUSC3 in prostate cancer cell lines. EGFR mRNA expression was measured by qRT-PCR. Data was normalized to HPRT1 expression as housekeeping gene while EGFR expression in shscr cells was set as one. Error bars represent the standard deviation of the mean (n=3). There are no significant differences in expression of EGFR in shTUSC3 cells compared to shscr cells.

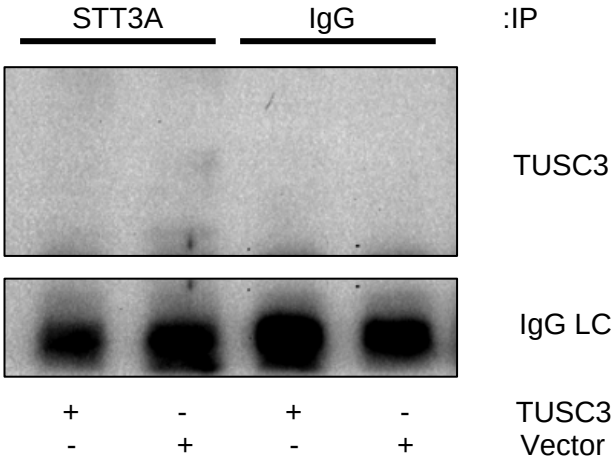

Supplementary Figure 3 (referring to 3.2.1): Co-Immunoprecipitation of TUSC3 with STT3A failed. HEK293 cells were transiently transfected with a TUSC3 expressing vector or the empty vector, respectively. Though, it was not possible to precipitate TUSC3 with 2µg of antibodies against STT3A.

Table 9: Quantitation of Western Blot images provided in this thesis

Values for Figure 11 and Figure 12, right panels:

Volume (Int)	DU145 shscr	DU145 shTUSC3	PC3 shscr	PC3 shTUSC3	HEK293 vector	HEK293 ovTUSC3
TUSC3 (upper band)	1807176	1234320	394267	283803	382580	869736
TUSC3 (lower band)	1932882	1273080	850282	287547	428956	957516
TUSC3 (sum)	3740058	2507400	1244549	571350	811536	1827252
β-Actin	3065760	2663893	3357945	1506750	821926	894739

Rel. Quant. TUSC3:β-Actin	DU145 shscr	DU145 shTUSC3	PC3 shscr	PC3 shTUSC3	HEK293 vector	HEK293 ovTUSC3
TUSC3 (upper band)	0,5895	0,4634	0,1174	0,1884	0,4655	0,9721
TUSC3 (lower band)	0,6305	0,4779	0,2532	0,1908	0,5219	1,0702
TUSC3 (sum)	1,2199	0,9413	0,3706	0,3792	0,9874	2,0422
β-Actin	1,0000	1,0000	1,0000	1,0000	1,0000	1,0000

Values for Figure 16 (P-AKT, AKT & β-Actin), Figure 17 (EGFR & β-Tubulin) and Figure 21 (E-cadherin & β-Actin):

Volume (Int)	10% serum				72h serum starvation			
	DU145 shscr	DU145 shTUSC3	PC3 shscr	PC3 shTUSC3	DU145 shscr	DU145 shTUSC3	PC3 shscr	PC3 shTUSC3
E-Cadherin	4184024	29978181	930852	644904	4655820	35949212	824466	1487318
P-AKT	2792920	6282084	15898220	37166376	490360	490464	9203056	28208946
T-AKT	17127942	11409312	5970009	7884141	7788975	7085226	4263957	6944976
β-Actin	50495068	43587387	52398736	57039320	17489524	49096892	61112318	77418098
EGFR	140112	339724	231392	161112	113540	523516	97720	111496
β-Tubulin	1854296	1720080	2296156	2511264	1878135	2481134	1846952	2162592

Rel. Quant.	10% serum				72h serum starvation			
	DU145 shscr	DU145 shTUSC3	PC3 shscr	PC3 shTUSC3	DU145 shscr	DU145 shTUSC3	PC3 shscr	PC3 shTUSC3
E-Cadherin	0,0829	0,6878	0,0178	0,0113	0,2662	0,7322	0,0135	0,0192
P-AKT	0,0553	0,1441	0,3034	0,6516	0,0280	0,0100	0,1506	0,3644
T-AKT	0,3392	0,2618	0,1139	0,1382	0,4454	0,1443	0,0698	0,0897
β-Actin	1,0000	1,0000	1,0000	1,0000	1,0000	1,0000	1,0000	1,0000
EGFR	0,0756	0,1975	0,1008	0,0642	0,0605	0,2110	0,0529	0,0516
β-Tubulin	1,0000	1,0000	1,0000	1,0000	1,0000	1,0000	1,0000	1,0000

6 References

Bae, K. M., Parker, N. N., Dai, Y., Vieweg, J., & Siemann, D. W. (2011). E-cadherin plasticity in prostate cancer stem cell invasion. *Am J Cancer Res, 1*(1), 71-84.

Bashyam, M. D., Bair, R., Kim, Y. H., Wang, P., Hernandez-Boussard, T., Karikari, C. A., . . . Pollack, J. R. (2005). Array-based comparative genomic hybridization identifies localized DNA amplifications and homozygous deletions in pancreatic cancer. *Neoplasia, 7*(6), 556-562.

Baumann, O., & Walz, B. (2001). Endoplasmic reticulum of animal cells and its organization into structural and functional domains. *Int Rev Cytol, 205*, 149-214.

Berridge, M. J. (2002). The endoplasmic reticulum: a multifunctional signaling organelle. *Cell Calcium, 32*(5-6), 235-249.

Boelens, J., Lust, S., Offner, F., Bracke, M. E., & Vanhoecke, B. W. (2007). Review. The endoplasmic reticulum: a target for new anticancer drugs. *In Vivo, 21*(2), 215-226.

Bookstein, R., Rio, P., Madreperla, S. A., Hong, F., Allred, C., Grizzle, W. E., & Lee, W. H. (1990). Promoter deletion and loss of retinoblastoma gene expression in human prostate carcinoma. *Proc Natl Acad Sci U S A, 87*(19), 7762-7766.

Bova, G. S., MacGrogan, D., Levy, A., Pin, S. S., Bookstein, R., & Isaacs, W. B. (1996). Physical mapping of chromosome 8p22 markers and their homozygous deletion in a metastatic prostate cancer. *Genomics, 35*(1), 46-54.

Bull, V. H., & Thiede, B. (2012). Proteome analysis of tunicamycin-induced ER stress. *Electrophoresis, 33*(12), 1814-1823.

Cavallaro, U., & Christofori, G. (2001). Cell adhesion in tumor invasion and metastasis: loss of the glue is not enough. *Biochim Biophys Acta, 1552*(1), 39-45.

Chen, H., Paradies, N. E., Fedor-Chaiken, M., & Brackenbury, R. (1997). E-cadherin mediates adhesion and suppresses cell motility via distinct mechanisms. *J Cell Sci, 110 (Pt 3)*, 345-356.

Cher, M. L., Bova, G. S., Moore, D. H., Small, E. J., Carroll, P. R., Pin, S. S., . . . Jensen, R. H. (1996). Genetic alterations in untreated metastases and androgen-independent prostate cancer detected by comparative genomic hybridization and allelotyping. *Cancer Res, 56*(13), 3091-3102.

Contessa, J. N., Bhojani, M. S., Freeze, H. H., Rehemtulla, A., & Lawrence, T. S. (2008). Inhibition of N-linked glycosylation disrupts receptor tyrosine kinase signaling in tumor cells. *Cancer Res, 68*(10), 3803-3809.

Contessa, J. N., Bhojani, M. S., Freeze, H. H., Ross, B. D., Rehemtulla, A., & Lawrence, T. S. (2010). Molecular imaging of N-linked glycosylation suggests glycan biosynthesis is a novel target for cancer therapy. *Clin Cancer Res, 16*(12), 3205-3214.

Csala, M., Kereszturi, E., Mandl, J., & Banhegyi, G. (2012). The endoplasmic reticulum as the extracellular space inside the cell: role in protein folding and glycosylation. *Antioxid Redox Signal, 16*(10), 1100-1108.

Dall'olio, F. (1996). Protein glycosylation in cancer biology: an overview. *Clin Mol Pathol, 49*(3), M126-135.

Davies, M. P., Barraclough, D. L., Stewart, C., Joyce, K. A., Eccles, R. M., Barraclough, R., . . . Sibson, D. R. (2008). Expression and splicing of the unfolded protein response gene XBP-1 are significantly associated with clinical outcome of endocrine-treated breast cancer. *Int J Cancer, 123*(1), 85-88.

Du, K., Herzig, S., Kulkarni, R. N., & Montminy, M. (2003). TRB3: a tribbles homolog that inhibits Akt/PKB activation by insulin in liver. *Science, 300*(5625), 1574-1577.

El Gammal, A. T., Bruchmann, M., Zustin, J., Isbarn, H., Hellwinkel, O. J., Kollermann, J., . . . Schlomm, T. (2010). Chromosome 8p deletions and 8q gains are associated with tumor progression and poor prognosis in prostate cancer. *Clin Cancer Res, 16*(1), 56-64.

Fang, M., Shen, Z., Huang, S., Zhao, L., Chen, S., Mak, T. W., & Wang, X. (2010). The ER UDPase ENTPD5 promotes protein N-glycosylation, the Warburg effect, and proliferation in the PTEN pathway. *Cell, 143*(5), 711-724.

Fu, Y., Wey, S., Wang, M., Ye, R., Liao, C. P., Roy-Burman, P., & Lee, A. S. (2008). Pten null prostate tumorigenesis and AKT activation are blocked by targeted knockout of ER chaperone GRP78/BiP in prostate epithelium. *Proc Natl Acad Sci U S A, 105*(49), 19444-19449.

Gallick, G. E., Corn, P. G., Zurita, A. J., & Lin, S. H. (2012). Small-molecule protein tyrosine kinase inhibitors for the treatment of metastatic prostate cancer. *Future Med Chem, 4*(1), 107-119.

Gao, A. C., Lou, W., Dong, J. T., & Isaacs, J. T. (1997). CD44 is a metastasis suppressor gene for prostatic cancer located on human chromosome 11p13. *Cancer Res, 57*(5), 846-849.

Garshasbi, M., Hadavi, V., Habibi, H., Kahrizi, K., Kariminejad, R., Behjati, F., . . . Kuss, A. W. (2008). A defect in the TUSC3 gene is associated with autosomal recessive mental retardation. *Am J Hum Genet, 82*(5), 1158-1164.

Garshasbi, M., Kahrizi, K., Hosseini, M., Nouri Vahid, L., Falah, M., Hemmati, S., . . . Kuss, A. W. (2011). A novel nonsense mutation in TUSC3 is responsible for non-syndromic autosomal recessive mental retardation in a consanguineous Iranian family. *Am J Med Genet A, 155A*(8), 1976-1980.

Gu, F., Nguyen, D. T., Stuible, M., Dube, N., Tremblay, M. L., & Chevet, E. (2004). Protein-tyrosine phosphatase 1B potentiates IRE1 signaling during endoplasmic reticulum stress. *J Biol Chem, 279*(48), 49689-49693.

Hakomori, S. (2002). Glycosylation defining cancer malignancy: new wine in an old bottle. *Proc Natl Acad Sci U S A, 99*(16), 10231-10233.

Hanahan, D., & Weinberg, R. A. (2000). The hallmarks of cancer. *Cell, 100*(1), 57-70.

Hanahan, D., & Weinberg, R. A. (2011). Hallmarks of cancer: the next generation. *Cell, 144*(5), 646-674.

Helenius, A., & Aebi, M. (2001). Intracellular functions of N-linked glycans. *Science, 291*(5512), 2364-2369.

Hermel, E., & Klapstein, K. D. (2011). A possible mechanism for maintenance of the deleterious allele of human CASPASE-12. *Med Hypotheses, 77*(5), 803-806.

Higa, G. M., & Abraham, J. (2007). Lapatinib in the treatment of breast cancer. *Expert Rev Anticancer Ther, 7*(9), 1183-1192.

Hornbeck, P. V., Kornhauser, J. M., Tkachev, S., Zhang, B., Skrzypek, E., Murray, B., . . . Sullivan, M. (2012). PhosphoSitePlus: a comprehensive resource for investigating the structure and function of experimentally determined post-translational modifications in man and mouse. *Nucleic Acids Res, 40*(Database issue), D261-270.

Iyer, R., & Bharthuar, A. (2010). A review of erlotinib--an oral, selective epidermal growth factor receptor tyrosine kinase inhibitor. *Expert Opin Pharmacother, 11*(2), 311-320.

Jamaluddin, M. F., Bailey, U. M., Tan, N. Y., Stark, A. P., & Schulz, B. L. (2011). Polypeptide binding specificities of Saccharomyces cerevisiae oligosaccharyltransferase accessory proteins Ost3p and Ost6p. *Protein Sci, 20*(5), 849-855.

Janik, M. E., Litynska, A., & Vereecken, P. (2010). Cell migration-the role of integrin glycosylation. *Biochim Biophys Acta, 1800*(6), 545-555.

Jemal, A., Bray, F., Center, M. M., Ferlay, J., Ward, E., & Forman, D. (2011). Global cancer statistics. *CA Cancer J Clin, 61*(2), 69-90.

Kaighn, M. E., Narayan, K. S., Ohnuki, Y., Lechner, J. F., & Jones, L. W. (1979). Establishment and characterization of a human prostatic carcinoma cell line (PC-3). *Invest Urol, 17*(1), 16-23.

Karaoglu, D., Kelleher, D. J., & Gilmore, R. (1995). Functional characterization of Ost3p. Loss of the 34-kD subunit of the Saccharomyces cerevisiae oligosaccharyltransferase results in biased underglycosylation of acceptor substrates. *J Cell Biol, 130*(3), 567-577.

Karaoglu, D., Kelleher, D. J., & Gilmore, R. (1997). The highly conserved Stt3 protein is a subunit of the yeast oligosaccharyltransferase and forms a subcomplex with Ost3p and Ost4p. *J Biol Chem, 272*(51), 32513-32520.

Kebache, S., Cardin, E., Nguyen, D. T., Chevet, E., & Larose, L. (2004). Nck-1 antagonizes the endoplasmic reticulum stress-induced inhibition of translation. *J Biol Chem, 279*(10), 9662-9671.

Kekeeva, T. V., Popova, O. P., Shegai, P. V., Alekseev, B., Adnreeva, I., Zaletaev, D. V., & Nemtsova, M. V. (2007). [Abberant methylation of p16, HIC1, N33 and GSTP1 genes in tumor epitelium and tumor-associated stromal cells of prostate cancer]. *Mol Biol (Mosk), 41*(1), 79-85.

Kelleher, D. J., & Gilmore, R. (2006). An evolving view of the eukaryotic oligosaccharyltransferase. *Glycobiology, 16*(4), 47R-62R.

Kelleher, D. J., Karaoglu, D., Mandon, E. C., & Gilmore, R. (2003). Oligosaccharyltransferase isoforms that contain different catalytic STT3 subunits have distinct enzymatic properties. *Mol Cell, 12*(1), 101-111.

Knauer, R., & Lehle, L. (1999). The oligosaccharyltransferase complex from yeast. *Biochim Biophys Acta, 1426*(2), 259-273.

Knudson, A. G., Jr. (1971). Mutation and cancer: statistical study of retinoblastoma. *Proc Natl Acad Sci U S A, 68*(4), 820-823.

Laemmli, U. K. (1970). Cleavage of structural proteins during the assembly of the head of bacteriophage T4. *Nature, 227*(5259), 680-685.

Lin, W., & Popko, B. (2009). Endoplasmic reticulum stress in disorders of myelinating cells. *Nat Neurosci, 12*(4), 379-385.

Loddo, S., Parisi, V., Doccini, V., Filippi, T., Bernardini, L., Brovedani, P., . . . Battaglia, A. (2013). Homozygous deletion in TUSC3 causing syndromic intellectual disability: A new patient. *Am J Med Genet A*.

Matsuyama, H., Pan, Y., Yoshihiro, S., Kudren, D., Naito, K., Bergerheim, U. S., & Ekman, P. (2003). Clinical significance of chromosome 8p, 10q, and 16q deletions in prostate cancer. *Prostate, 54*(2), 103-111.

McKeage, K. (2012). Docetaxel: a review of its use for the first-line treatment of advanced castration-resistant prostate cancer. *Drugs, 72*(11), 1559-1577.

Mhamdi, O., Kharrat, M., Mrad, R., Maazoul, F., & Chaabouni Bouhamed, H. (2011). Non-syndromic autosomal recessive mental retardation in Tunisian families : exclusion of GRIK2 and TUSC3 genes. *Tunis Med, 89*(5), 479-484.

Moenner, M., Pluquet, O., Bouchecareilh, M., & Chevet, E. (2007). Integrated endoplasmic reticulum stress responses in cancer. *Cancer Res, 67*(22), 10631-10634.

Mohorko, E., Glockshuber, R., & Aebi, M. (2011). Oligosaccharyltransferase: the central enzyme of N-linked protein glycosylation. *J Inherit Metab Dis, 34*(4), 869-878.

Morin, M. J., & Bernacki, R. J. (1983). Biochemical effects and therapeutic potential of tunicamycin in murine L1210 leukemia. *Cancer Res, 43*(4), 1669-1674.

Nakano, M., Takahashi, H., Shiraishi, T., Lu, T., Furusato, M., Wakui, S., & Hano, H. (2008). Prediction of clinically insignificant prostate cancer by detection of allelic imbalance at 6q, 8p and 13q. *Pathol Int, 58*(7), 415-420.

Nguyen, D. T., Kebache, S., Fazel, A., Wong, H. N., Jenna, S., Emadali, A., . . . Chevet, E. (2004). Nck-dependent activation of extracellular signal-regulated kinase-1 and regulation of cell survival during endoplasmic reticulum stress. *Mol Biol Cell, 15*(9), 4248-4260.

Pils, D., Horak, P., Gleiss, A., Sax, C., Fabjani, G., Moebus, V. J., . . . Krainer, M. (2005). Five genes from chromosomal band 8p22 are significantly down-regulated in ovarian carcinoma: N33 and EFA6R have a potential impact on overall survival. *Cancer, 104*(11), 2417-2429.

Pils, D., Horak, P., Vanhara, P., Anees, M., Petz, M., Alfanz, A., . . . Krainer, M. (2012). Methylation status of TUSC3 is a prognostic factor in ovarian cancer. *Cancer*.

Pils, D., Horak, P., Vanhara, P., Anees, M., Petz, M., Alfanz, A., . . . Krainer, M. (2013). Methylation status of TUSC3 is a prognostic factor in ovarian cancer. *Cancer, 119*(5), 946-954.

Pinho, S. S., Seruca, R., Gartner, F., Yamaguchi, Y., Gu, J., Taniguchi, N., & Reis, C. A. (2011). Modulation of E-cadherin function and dysfunction by N-glycosylation. *Cell Mol Life Sci, 68*(6), 1011-1020.

Pourmand, G., Ziaee, A. A., Abedi, A. R., Mehrsai, A., Alavi, H. A., Ahmadi, A., & Saadati, H. R. (2007). Role of PTEN gene in progression of prostate cancer. *Urol J, 4*(2), 95-100.

Rahmani, M., Davis, E. M., Crabtree, T. R., Habibi, J. R., Nguyen, T. K., Dent, P., & Grant, S. (2007). The kinase inhibitor sorafenib induces cell death through a process involving induction of endoplasmic reticulum stress. *Mol Cell Biol, 27*(15), 5499-5513.

Ross, R., Bernstein, L., Judd, H., Hanisch, R., Pike, M., & Henderson, B. (1986). Serum testosterone levels in healthy young black and white men. *J Natl Cancer Inst, 76*(1), 45-48.

Ross, R. K., Bernstein, L., Lobo, R. A., Shimizu, H., Stanczyk, F. Z., Pike, M. C., & Henderson, B. E. (1992). 5-alpha-reductase activity and risk of prostate cancer among Japanese and US white and black males. *Lancet, 339*(8798), 887-889.

Ruijter, E., van de Kaa, C., Miller, G., Ruiter, D., Debruyne, F., & Schalken, J. (1999). Molecular genetics and epidemiology of prostate carcinoma. *Endocr Rev, 20*(1), 22-45.

Samali, A., Fitzgerald, U., Deegan, S., & Gupta, S. (2010). Methods for monitoring endoplasmic reticulum stress and the unfolded protein response. *Int J Cell Biol, 2010*, 830307.

Sarkar, F. H., Sakr, W., Li, Y. W., Macoska, J., Ball, D. E., & Crissman, J. D. (1992). Analysis of retinoblastoma (RB) gene deletion in human prostatic carcinomas. *Prostate, 21*(2), 145-152.

Sarker, D., Reid, A. H., Yap, T. A., & de Bono, J. S. (2009). Targeting the PI3K/AKT pathway for the treatment of prostate cancer. *Clin Cancer Res, 15*(15), 4799-4805.

Schulz, B. L., & Aebi, M. (2009). Analysis of glycosylation site occupancy reveals a role for Ost3p and Ost6p in site-specific N-glycosylation efficiency. *Mol Cell Proteomics, 8*(2), 357-364.

Schulz, B. L., Stirnimann, C. U., Grimshaw, J. P., Brozzo, M. S., Fritsch, F., Mohorko, E., . . . Aebi, M. (2009). Oxidoreductase activity of oligosaccharyltransferase subunits Ost3p and Ost6p defines site-specific glycosylation efficiency. *Proc Natl Acad Sci U S A, 106*(27), 11061-11066.

Schwartz, G. G., & Hulka, B. S. (1990). Is vitamin D deficiency a risk factor for prostate cancer? (Hypothesis). *Anticancer Res, 10*(5A), 1307-1311.

Schwarz, M., Knauer, R., & Lehle, L. (2005). Yeast oligosaccharyltransferase consists of two functionally distinct sub-complexes, specified by either the Ost3p or Ost6p subunit. *FEBS Lett, 579*(29), 6564-6568.

Sos, M. L., Koker, M., Weir, B. A., Heynck, S., Rabinovsky, R., Zander, T., . . . Thomas, R. K. (2009). PTEN loss contributes to erlotinib resistance in EGFR-mutant lung cancer by activation of Akt and EGFR. *Cancer Res, 69*(8), 3256-3261.

Stone, K. R., Mickey, D. D., Wunderli, H., Mickey, G. H., & Paulson, D. F. (1978). Isolation of a human prostate carcinoma cell line (DU 145). *Int J Cancer, 21*(3), 274-281.

Suh, D. H., Kim, M. K., Kim, H. S., Chung, H. H., & Song, Y. S. (2012). Unfolded protein response to autophagy as a promising druggable target for anticancer therapy. *Ann N Y Acad Sci, 1271*, 20-32.

Summers, S. A., Garza, L. A., Zhou, H., & Birnbaum, M. J. (1998). Regulation of insulin-stimulated glucose transporter GLUT4 translocation and Akt kinase activity by ceramide. *Mol Cell Biol, 18*(9), 5457-5464.

Szegezdi, E., Logue, S. E., Gorman, A. M., & Samali, A. (2006). Mediators of endoplasmic reticulum stress-induced apoptosis. *EMBO Rep, 7*(9), 880-885.

Taylor, B. S., Schultz, N., Hieronymus, H., Gopalan, A., Xiao, Y., Carver, B. S., . . . Gerald, W. L. (2010). Integrative genomic profiling of human prostate cancer. *Cancer Cell, 18*(1), 11-22.

Teske, B. F., Fusakio, M. E., Zhou, D., Shan, J., McClintick, J. N., Kilberg, M. S., & Wek, R. C. (2013). CHOP Induces Activating Transcription Factor 5 (ATF5) to Trigger Apoptosis in Response to Perturbations in Protein Homeostasis. *Mol Biol Cell*.

Tricoli, J. V., Gumerlock, P. H., Yao, J. L., Chi, S. G., D'Souza, S. A., Nestok, B. R., & deVere White, R. W. (1996). Alterations of the retinoblastoma gene in human prostate adenocarcinoma. *Genes Chromosomes Cancer, 15*(2), 108-114.

Troutman, S. M., Price, D. K., & Figg, W. D. (2010). Prostate cancer genomic signature offers prognostic value. *Cancer Biol Ther, 10*(11), 1079-1080.

Tsai, Y. C., & Weissman, A. M. (2010). The Unfolded Protein Response, Degradation from Endoplasmic Reticulum and Cancer. *Genes Cancer, 1*(7), 764-778.

Vanhara, P., Horak, P., Pils, D., Anees, M., Petz, M., Gregor, W., . . . Krainer, M. (2013). Loss of the oligosaccharyl transferase subunit TUSC3 promotes proliferation and migration of ovarian cancer cells. *Int J Oncol, 42*(4), 1383-1389.

Vlietstra, R. J., van Alewijk, D. C., Hermans, K. G., van Steenbrugge, G. J., & Trapman, J. (1998). Frequent inactivation of PTEN in prostate cancer cell lines and xenografts. *Cancer Res, 58*(13), 2720-2723.

Wellen, K. E., & Thompson, C. B. (2012). A two-way street: reciprocal regulation of metabolism and signalling. *Nat Rev Mol Cell Biol, 13*(4), 270-276.

Wu, A. H., Whittemore, A. S., Kolonel, L. N., John, E. M., Gallagher, R. P., West, D. W., . . . Paffenbarger, R. S., Jr. (1995). Serum androgens and sex hormone-binding globulins in relation to lifestyle factors in older African-American, white, and Asian men in the United States and Canada. *Cancer Epidemiol Biomarkers Prev, 4*(7), 735-741.

Yuan, T. L., & Cantley, L. C. (2008). PI3K pathway alterations in cancer: variations on a theme. *Oncogene, 27*(41), 5497-5510.

Zhang, H., Loriaux, P., Eng, J., Campbell, D., Keller, A., Moss, P., . . . Aebersold, R. (2006). UniPep--a database for human N-linked glycosites: a resource for biomarker discovery. *Genome Biol, 7*(8), R73.

Zhao, Y., Sato, Y., Isaji, T., Fukuda, T., Matsumoto, A., Miyoshi, E., . . . Taniguchi, N. (2008). Branched N-glycans regulate the biological functions of integrins and cadherins. *FEBS J, 275*(9), 1939-1948.

Zhou, H., & Clapham, D. E. (2009). Mammalian MagT1 and TUSC3 are required for cellular magnesium uptake and vertebrate embryonic development. *Proc Natl Acad Sci U S A, 106*(37), 15750-15755.

List of Abbreviations

5-alphaR	5-alpha-reductase
8p	Short arm of chromosome 8
AKT	Protein Kinase B (PKB)
AR	Androgen receptor
ARE	Androgen responsive element
BSA	Bovine serum albumine
CHOP	C/EBP homologous protein
cDNA	complementary deoxyribonucleic acid
ConA	Concanavalin A
DHT	Dihydrotestosteron
DMEM	Dulbecco’s modified Eagle's medium
DMSO	Dimethyl sulfoxide
DTT	Dithiothreitol
ECM	Extracellular matrix
EDTA	Ethylenediaminetetraacetic acid
EGFP	Enhanced green fluorescence protein
EGFR	Epithelial growth factor
ENTPD5	Ectonucleoside triphosphate diphosphohydrolase 5
ER	Endoplasmic reticulum
ERAD	Endoplasmic-reticulum-associated protein degradation
FBS	Fetal bovine serum
FDA	Food and Drug Administration
FIGO	International Federation of Gynecology and Obstetrics
GlcNAc	N-Acetylglucosamine
GLUT	Glucose transporter
HEK293	Human Embryonic Kidney 293
HPRT1	Hypoxanthine-guanine phosphoribosyltransferase 1

HRP	Horseradish peroxidase
IgG	Immunglobulin G
IGFR-1	Insulin growth factor receptor
Luc	Luciferase
MagT1	Magnesium Transporter 1
mRNA	messenger ribonucleic acid
mTORC	Mammalian target of rapamycin complex
OST	Oligosaccharyltransferase
PAGE	Polyacrylamid gelelectrophoresis
PBS	Phosphate buffered saline
PCa	Prostate cancer
PCR	polymerase chain reaction
PHA	Phytohaemagglutinin
PI3K	Phosphoinositide 3-kinase
PIP2	Phosphatidylinositol 4,5-bisphosphate
PIP3	Phosphatidylinositol (3,4,5)-trisphosphate
PKB	Protein kinase B
PNGase F	Peptide -N-Glycosidase F
PSA	Prostate specific antigen
PTEN	Phosphatase and tensin homolog
qRT-PCR	quantitative realtime polymerase chain reaction
Rb-1	Retinoblastoma
RIPA	Radioimmunoprecipitation assay
ROS	Reactive oxygen species
RPMI	Roswell Park Memorial Institute medium
RTK	Receptor tyrosine kinase
SDS	Sodium dodecyl sulfate
shRNA	short hairpin ribonucleic acid

T	Testosteron
TAE	Tris base, acetic acid and EDTA
TP53	Tumor protein 53
TSG	Tumor suppressor gene
TUSC3	Tumor suppressor candidate 3
UDP	Uridindiphosphat
UPR	Unfolded protein response
VEGF	Vascular endothelial growth factor
XBP1	X-box binding protein 1

List of Figures

"I was endeavoring to find all the image rights owners and obtaining their approval to use the images in the present work. If an infringement of copyright exists anyway, I would ask for notice."

List of Tables

Acknowledgements

Foremost, I need to thank Prof. Michael Krainer for allowing me to join his group, giving me the possibility to work in an outstanding place and scientific atmosphere. I thank my supervisor Dr. Peter Horak for giving an innocent biologist a chance to do his first steps in science and never losing faith in me or my work at times when I already did.

I want to thank Prof. Natale-Erwin Ivessa for accepting to take on my thesis and contributing to it with his knowledge and expertise.

It always was and will remain being a big pleasure to share a laboratory with Maximilian Marhold. I am deeply thankful for his presence, motivation and friendship.

Thanks goes also to my other lab members and co-workers: Maria König, for her kindness and always open-ears; Dr. Mariam Anees, for her unforgettable maternal care; Andrea Schanzer for her, measured on her nerves, infinite patience with someone like me; Bettina Savarese-Brenner, for showing me that it is possible to survive a diploma thesis in our group; Dr. Christof Lemberger, for encouraging and challenging myself, and Dr. Petr Vanhara, for teaching me some tips and tricks and to always look at the bright side of science/life. Barbara Ziegler, not only for opening me the door for almost half a year but especially for being such an inestimably spiritually and mentally support; Corinna Altenberger, for showing me that it is possible to leave work before darkness falls; Dr. Christoph Minichsdorfer for always let me have the cell culture hood without a struggle and any tears; and Dr. Gerwin Heller, for the certainty, that next to all the clinicians there is also one excellent biologist around. Birgit Steinmetz, for the many advices and even more decisions I wasn't able to make alone; and Nastasia Wilfinger, for all the joy and laughter which made work so much easier.

Just not forget to mention: Trang Le, Franz Rieder, Marie-Theres Kastner, Patricia Weiss, Clemens Pausz, Sebastian Dorn, Marlene Weinzierl, Dr. Karine Gonzales, Muriel Fisser, Anna Rommer, Katarina Steinleitner, Katharina Hartl, Daniela Hailos, Doz. Karin Nowikovsky, Shane Austin, Betül Kutay, Martin Schalling, and all the other people who turned the Anna Spiegel Research Building into more than just a working place.

Last but not least I am grateful for being blessed with a wonderful family and friends. I thank my parents for their unconditional support and generosity and my friends Dani, Tina, Conny, Moni, Jenny, Michi, Andi and Thomas for never forgot about me in the past years.

Curriculum Vitae

personal details

name:	Erwin TOMASICH
date of birth:	11. March 1987
place of birth:	Vienna
nationality:	Austria

education

1993-1997	Elementary School
	Sacré Coeur, Rennweg 31, 1030 Vienna
1997-2005	High School
	Geringerg. 2, 1110 Vienna
2006-2013	Studies of Biology at the University of Vienna specialization: Microbiology and Genetics with main focus on Molecular Microbiology

hands-on training

2007	Labor-Gruppenpraxis Bauer, Spitzauer & Partner
August-September	Department for Microbiology & Bacteriology
2010	St. Anna Children's Cancer Research Institute
February	Genetics of Leukemia, Group: Sabine Strehl, PhD
2011	Center for Integrative Bioinformatics Vienna, MFPL
July-August	Group: Prof. Arndt von Haeseler
2011-2013	Diploma thesis at the Medical University of Vienna,
	Clinic for Internal Medicine I, Group: Prof. Michael Krainer

oral presentation

2012	Biomania - The Student Scientific Conference on Biotechnology
April 13th	and Biomedicine 2012 in Brno, Czech Republic
2012	OrganoNET lecture
September 26th	Masaryk University, Czech Republic